2011

Performance Characteristics of Airlift Pumps with Vortex Induced by Tangential Fluid Injection

Jacob Riglin
Bucknell University

Performance Characteristics of Airlift Pumps

with Vortex Induced by Tangential Fluid Injection
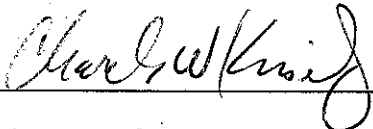
By

Jacob D. Riglin

A Thesis Submitted to the Honors Council

For Honors in Mechanical Engineering

May 9, 2011

Approved by:

_____

Adviser: Professor Charles Knisely

_____

Department Chair: Professor Charles Knisely

Acknowledgements

I would like to thank Professor Knisely for his offering me the opportunity to work on this project and for all his help and guidance; Tommy Caso for taking time out of his busy schedule to assist me on a whim; and Dan Johnson for his assistance in designing, manufacturing, and assembling components of the airlift pump and most of all for being patient with me, even when I made mistakes.

Table of Contents

List of Figures

List of Appendices

Appendix A: Part List

Appendix B: Calibration

Appendix C: Part Drawings

Appendix D: Air Flow Conversion

Appendix E: Data

Abstract

The effect of the swirl component of air injection on the performance of an airlift pump was examined experimentally. An airlift pump is a device that pumps a liquid or slurry using only gas injection. In this study, the liquid used was water and the injected gas was air. The effect of the air swirl was determined by measuring the water discharge from an airlift pump with an air injection nozzle in which the air flow had both axial and tangential components and then repeating the tests with a nozzle with only axial injection. The induced water flow was measured using an orifice meter in the supply pipeline. Tests were run for air pressures ranging from 10 to 30 pounds per square inch, gauge (psig), at flow rates from 5 standard cubic feet per minute (scfm) up the maximum values attainable at the given pressure (usually in the range from 20 to 35 scfm). The nozzle with only axial injection produced a water flow rate that was equivalent to or better than that induced by the nozzle with swirl. The swirl component of air injection was found to be detrimental to pump performance for all but the smallest air injection flow rate. Optimum efficiency was found for air injection pressures of 10 psig to 15 psig.

In addition, the effect of using auxiliary tangential injection of water to create a swirl component in the riser before air injection on the overall capacity (*i.e.,* flow rate) and efficiency of the pump was examined. Auxiliary tangential water injection was found to have no beneficial effect on the pump capacity or performance in the present system.

1

Introduction

        Airlift pumps are pumps that operate using a gas (usually air) to pump a denser fluid

(usually a liquid or a slurry). In the current experiment, the gas was air and the liquid was water.

Airlift pumps operate in two-phase flow, meaning that the flow consists of simultaneous flow of

substances of two different phases. Three-phase flow is also attainable with airlift pumps, with

a solid, liquid, and gas being transported simultaneously. Airlift pumps have characteristics that

make them more desirable than mechanical pumps in a few specific applications. Since there

are no moving parts in an airlift pump, there is minimal wear, reducing the need for

maintenance (Finio, 2007). The lack of rotational impeller blades allows airlift pumps to be used

for dredging applications, such as removing sediment from a riverbed or a harbor, and

potentially for mining valuable minerals from the ocean floor. In addition, airlift pumps can be

used to transport corrosive, abrasive liquids that could also damage a mechanical pump (Clark

and Dabolt, 1986) and petroleum. Carbon dioxide driven airlift pumps were considered for use

in the BP oil spill that occurred on April 20, 2010 in the Gulf of Mexico (Knisely, 2010). The

drawback to using an airlift pump is that airlift pumps operate at significantly lower efficiencies

than mechanical pumps. The efficiency in the case of an airlift pump is defined as the ratio of

the output pumping power to the required input power. Airlift pumps will typically operate at

efficiencies ranging from 35% to 55% (Clark and Dabolt, 1986) while mechanical pumps operate

at much higher efficiencies, often above 70%. Low efficiencies associated with airlift pumps

result from the high slip ratio between the air and the water, resulting in a poor transfer of

momentum from the gas to the liquid. The shear and buoyant forces of the injected air acting

on the water tend to pull the water up the riser, or entrain the water. The pump riser should be

oriented perfectly vertical, to maximize the buoyant force generated by the air.

The airlift pump arrangements shown in Figure 1 are two common embodiments of the concept of using the shear and buoyant forces to pump a liquid. In both Figure 1a and 1b, the pumps lift water vertically from the point of air injection to the point of discharge from the riser. Typical airlift pump discharge characteristics for a one inch diameter pipe are shown in Figure 2. The volumetric flow rate of the water, shown on the ordinate in Figure 2, clearly depends upon the air injection flow rate, shown on the abscissa. The second independent parameter in Figure 2 is the submergence ratio which is defined as the ratio between the depth from free surface to the point of air injection (denoted by H) and the overall length of the pipe from the point of air injection to point of discharge (denoted by L). The submergence ratio (H/L) also has a strong effect on the discharge characteristics of an airlift pump. The discharge characteristics in Figure 2 are representative of the performance of airlift pumps, producing increased discharge with increasing submergence ratio for the same air injection rate.
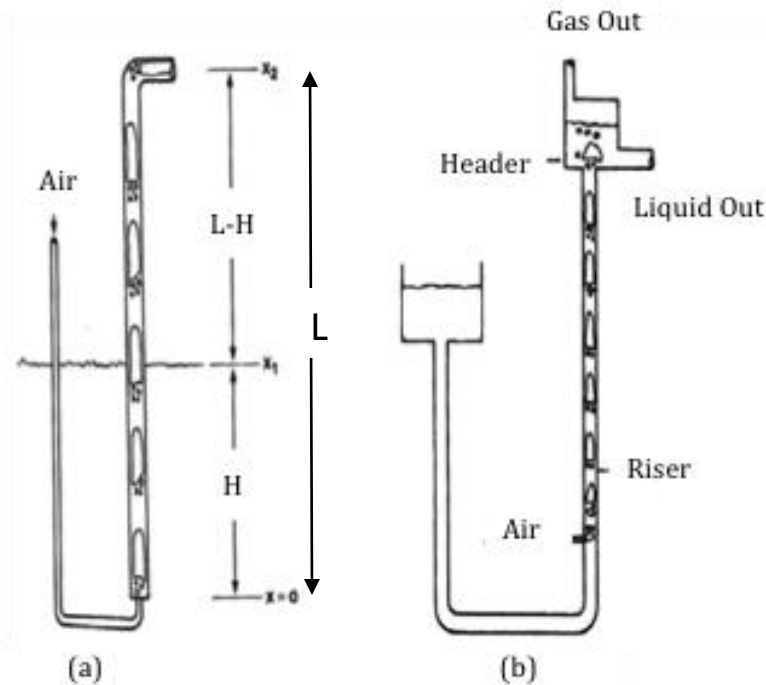
Figure 1: (a) Airlift tube immersed in well or vessel, and (b) U-tube arrangement of an airlift pump (from Clark and Dabolt,1986)
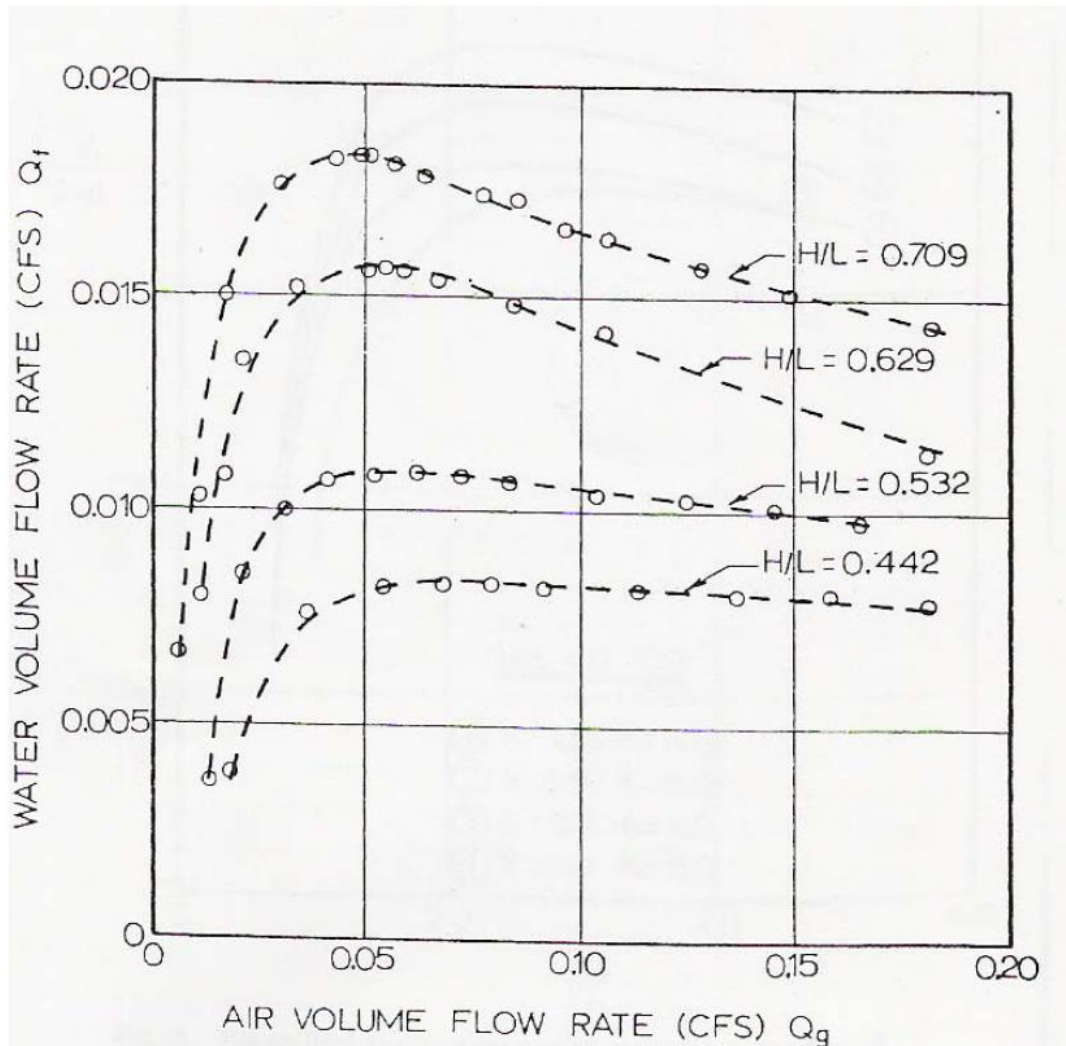
Figure 2: Water flow rate dependence on air flow rate at different submergence ratios (H/L) (Stenning and Martin, 1968)

Stenning and Martin (1968) examined the performance of airlift pumps detailing the effects of pipe diameter, submergence, and air flow rate. Increasing the air flow rate results in increasing water flow rate up to a point, after which the water flow rate levels off or may even decrease with a further increase in air flow rate. As already discussed in conjunction with the description of Figure 2, increasing the submergence ratio (H/L) leads to increased pump

discharge for the same air flow rate (but requires added input power if the submergence has increased due to the increased ambient pressure).

Stenning and Martin (1968) determined that larger piping diameters require less air flow to generate a given water flow rate; however, it was also noted that a larger diameter of piping would result in a substantially heavier weight of the pump, which would be a cause for concern if the system was intended for dredging, marine mining or mine dewatering applications. A larger, heavier system would be more difficult to constrain and support. Stenning and Martin also observed unsteadiness in two-phase flow. Pressure oscillations with a period of several seconds were observed, with the amplitude of the oscillations increasing as the water flow rate increased.

Francois, et al. (1996) compared experimental data from various airlift pump configurations with theoretical data. The starting point of their analysis was that the pumping power of any pump is the mass flow rate of water times the height it is being lifted (L-H) times the acceleration of gravity (*i.e.,* the rate of increase in potential energy). Further, the input power for the air injection is the mass flow rate of air times the energy input in the compressor (*i.e.,* the rate of enthalpy increase through the compressor), which in turn depends upon the required pressure to inject the air at a specified submergence. Thus, for a given pump at a fixed submergence (fixed lifting height and fixed input pressure) , they concluded that the overall efficiency of an airlift pump is proportional to the ratio of the water mass flow rate, Q_L, to the air mass flow rate, Q_G. In the remainder of the present study comparing airlift pumps with swirl flow to those without, efficiency will be considered to be the ratio of the water mass flow rate to the air mass flow rate since all tests are done at a constant submergence and constant lift.

Francois, et al (1996) also concluded that for each lift height, there is a minimum value of air flow that is required for any water flow rate to be achieved. The maximum capacity of an airlift pump at a given submergence ratio is the maximum liquid discharge (flow rate) that is attainable with the system configuration and with the specified injection gas. Figure 3 shows both water flow rate and efficiency as a function of air flow rate. It is important to note that the point of maximum efficiency and the point of maximum capacity occur at different values of air flow rate. Therefore, the ideal operating conditions would occur at a point between maximum efficiency and maximum capacity, since efficiency rapidly decreases after the point of maximum efficiency.

During two-phase flow airlift operation, the four different flow patterns shown in Figure 4 are commonly observed. The maximum efficiency and the maximum capacity of the pump are affected by these flow patterns, which in turn result from the combination of other factors including the submergence ratio, the major and minor losses in the piping system. Minor losses are losses that are caused by the geometry and setup of the pump, including elbows in the piping, contractions and expansions in piping, and entrances and exits of flows. Major losses result from pipe wall friction.

At small air flow rates, the system operates in the bubble flow regime (see Figure 4a). As the flow rate of the air increases, bubbles coalesce to form large bubbles that drive a "slug" of water up the pipe in the slug flow regime, shown in Figure 3b. As the airflow continues to increase, the large air bubbles become unstable, resulting in the churn flow shown in Figure 4c. The highest efficiency and maximum capacity, seen in Figure 3, occur near the slug flow/churn flow transition region during airlift operation. At large air flows, annular flow develops (Francois, et al., 1996).
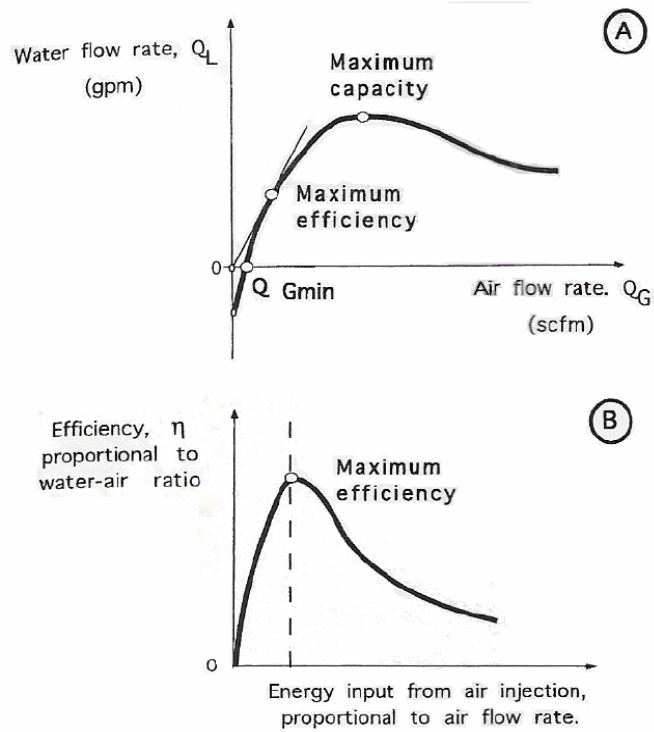
Figure 3: Dependence of water flow rate and efficiency on the air flow rate (Francois, et al., 1996).
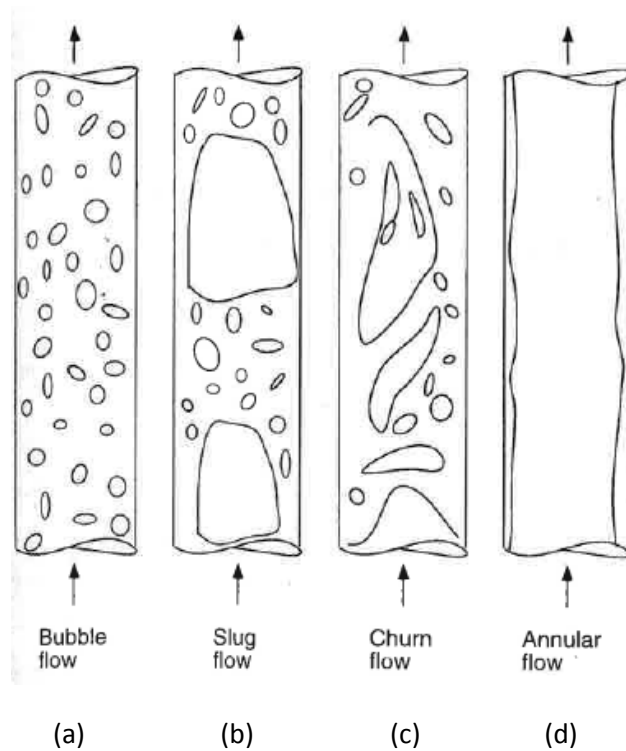
Figure 4: Two-phase flow patterns (Francois, et al., 1996).

Knisely and Finio (2010) presented data for airlift pumps with swirling air flow. In their experiments, 2" and 4" diameter interchangeable nozzles were used. The 2" nozzles had injection angles of 25°, 35°, and 45° from the vertical axis. The 4" nozzles they used had injection angles of 35° and differing numbers of helical paths for injected air flow. Figure 5 shows computer-generated images of their 4" nozzles. The effect of swirl was suggested by a corporate sponsor, and the different nozzle sizes permit fitting the pump to the requirements of each specified application.
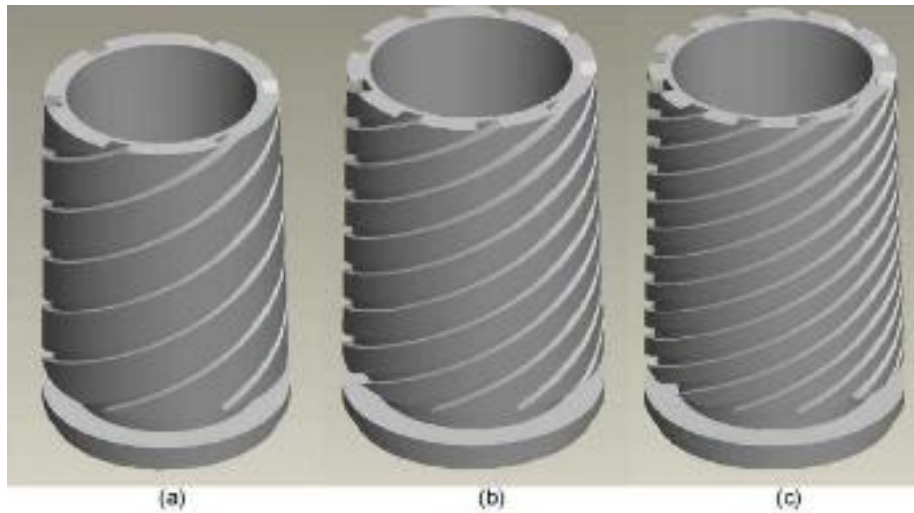
Figure 5: Interchangable 4" nozzles: (a) six helical paths, (b) nine helical paths, and (c) twelve helical paths (Knisely and Finio, 2010).

Knisely & Finio (2010) developed empirical equations for the efficiency of airlift pumps with no swirl from data found in Zenz (1993) and Pickert (1932), The two correlations they developed characterize the water flow rates and efficiencies expected in an airlift pump given values for the overall system and for properties of the substances driven during pump operation. Some of the published data, particularly the older data from Pickert (1932), pre-dated the delineation of flow regimes, shown in Figure 4. From the present day understanding of the correlation of performance with flow regime, it is safe to assume that the airlift pumps were in the slug flow regime or just transitioning into the churn flow regime. Knisely & Finio

(2010) introduced a normalized efficiency, formed by taking the ratio of the measured efficiency of the vortexing airlift pumps with swirl to the efficiency of comparable non-swirl airlift pumps (as determined from the two slightly different empirical correlations derived in their paper) to characterize the effect of swirl. From their resulting plot of normalized efficiency as a function of injected air flow rate, reproduced herein as Figure 6, Knisely & Finio (2010) concluded that adding a swirl component to the air flow enhances the performance of the pump only for small values of injected air flow, in the region where the efficiency of the vortexing airlift pump was greater than that for a comparable non-swirl pump, that is, where the normalized efficiency is greater than one.
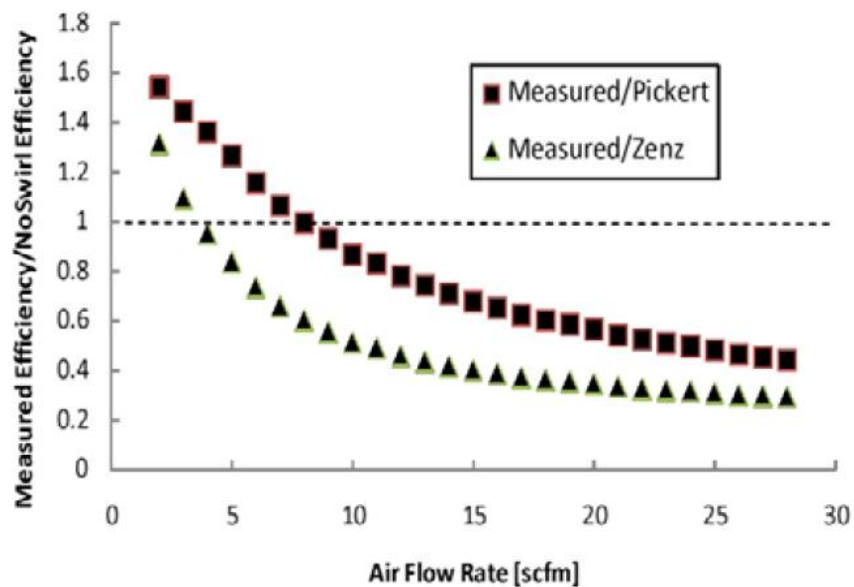
Figure 6: Effectiveness of swirl component of vortex-driven airlift pump with respect to non-swirl predictions based on correlations derived from the data of Zenz (1993) and Pickert (1932) (Knisely and Finio, 2010).

In addition to the effects of the swirled air flow, Knisely and Finio (2010) noted that the number of helical spirals had little effect on the performance of the airlift pump. As seen in Figure 7, there are no noticeable differences in the water flow rates for each helical configuration in the 4" diameter nozzles. Each nozzle leveled off at approximately the same

9

value for maximum capacity. In addition, injection angles of 25°, 35°, and 45° in the 2"

diameter nozzles did not yield a significant change in pump efficiency (Knisely and Finio, 2010).
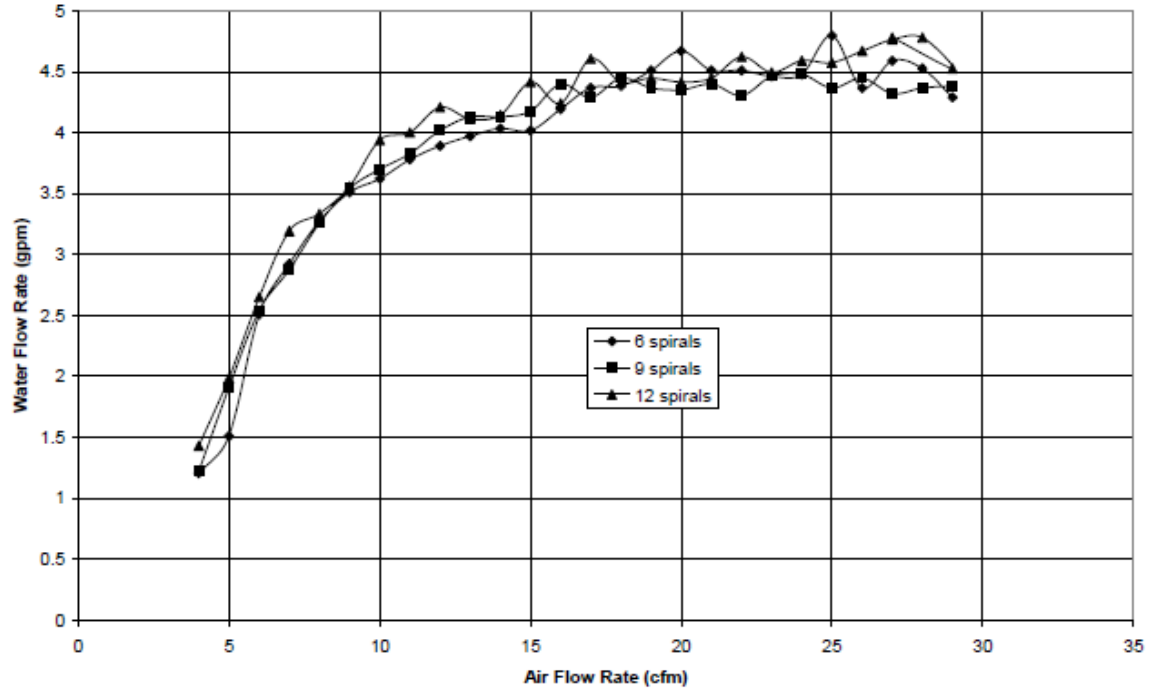
Figure 7: Water flow rate dependence on air flow rate for the four inch nozzles (Knisely and
Finio 2010).

Thesis Statement

The purpose of the experiments conducted in the present study is to determine how the swirl component of the injected air, or alternatively using auxiliary water flow to induce swirl in the water in the riser before the air injection point, affects the overall performance of an airlift pump. The performance of the pump will be evaluated for pressures ranging from 10 to 30 psig, using flow rates between 5 scfm and the maximum flow rate attainable at each pressure. Two interchangeable air injection nozzles will be used in the same airlift pump configuration. The first nozzle has helical spiral paths for the air injection, providing the air with both axial and tangential velocity components upon entry into the riser. The second nozzle has axially aligned channels along the perimeter of the nozzle, forcing the air to be injected with only an axial velocity. Previous experiments conducted by Knisely and Finio (2010) documented the airlift pump performance with the swirling air injection, but they did not undertake any measurements permitting direct comparison of the swirl and non-swirl nozzle configurations. Based on correlations for the performance of non-swirl airlift pumps (based on previously published data from multiple sources) derived in Knisely and Finio (2010), it is expected that the swirl component will result in minimal improvement to the overall efficiency and capacity of the pump. The goal of this project is to confirm or refute their predictions.

No previous research has been found that examined the effects of inducing water swirl in the riser by tangential injection of auxiliary water flow. As auxiliary water flow is driven into the system, a high pressure is expected to be present around the periphery of the inner pipe with a low pressure at the center of the pipe. The low pressure is expected to induce a greater axial water flow rate, thus increasing the efficiency of the pump.

Experiment & Methods

To determine the overall system performance, measurements of the primary water flow rate, auxiliary water flow rate (when used), and air flow rate were made. The auxiliary water flow is the component of water flow that is being injected into the riser before pump in order to generate swirl in the riser before air injection. A closed-loop piping system was used. Figure 8 shows the system configuration with key dimensions noted. Data on the numbered components with description, manufacturer, and model number are provided in Appendix A.
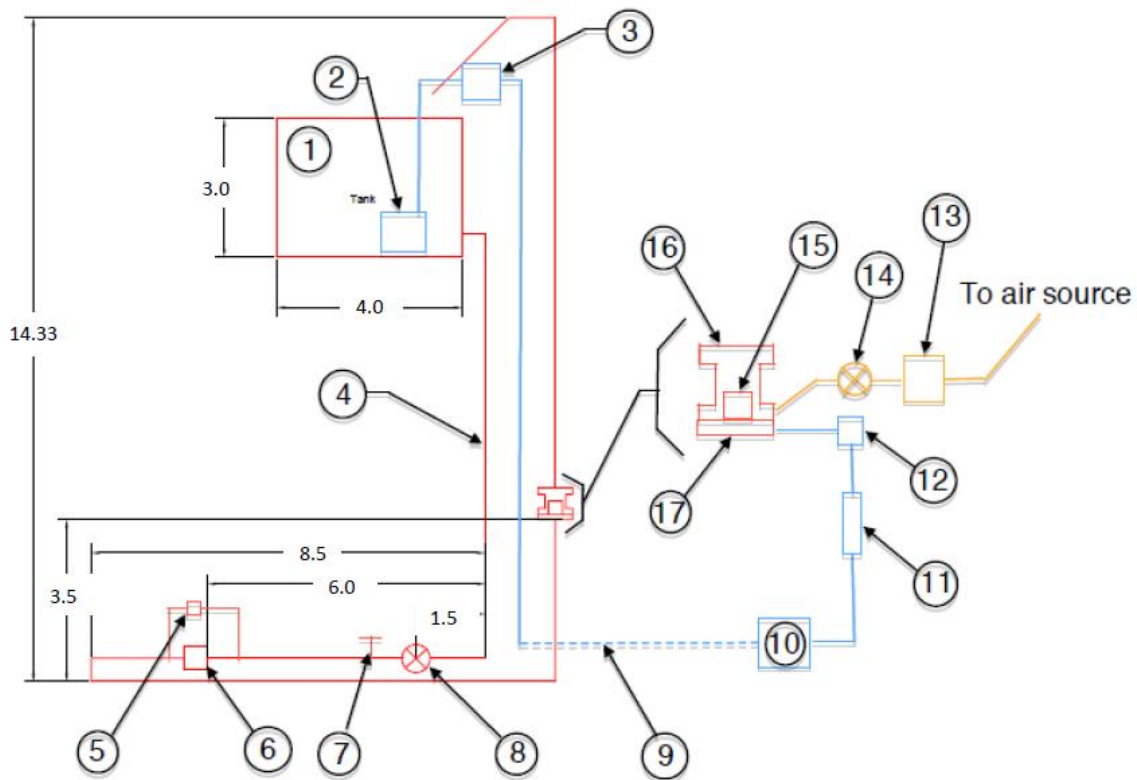
Figure 8: System diagram of the airlift pump. Red denotes primary water delivery piping, blue denotes the auxiliary water delivery piping, and orange denotes the air flow delivery piping. The primary water delivery piping schematic is to scale. Units that are displayed are in feet.

The compressed air supply available in the Fluids Lab, located in the basement of Dana Engineering, was used to supply air to the nozzle (#15). A high-pressure hose connected the supply valve to the air injection point. A control valve (#14) and an air rotameter (#13) were

placed in the main line to control and measure the air flow at the air injection point. The shutoff

valve was placed between the air rotameter and the air injection point to prevent the back flow

of water into the air rotameter and hosing while the pump is idle.

The primary water flow is drawn through the tank outlet and then through the

downcomer pipe. Pressure taps (one diameter and one-half diameter distances upstream and

downstream, respectively) were placed on either side of the orifice and were attached to a

differential pressure transducer (#5). The orifice was calibrated by recording the pressure

difference, in inches H_2O, across the orifice plate (#6). Simultaneously, discharge water at the

exit was collected in a bucket over a measured time. Weighing the contents of the bucket

permitted determination of the mass flow rate. There is a positive, linear correlation between

the pressure drop over the orifice and the square of the mass flow rate of the water. A

calibration plot was generated and the equation of the best linear fit was determined for the

calibration data. See Appendix B for further details on the calibration of the Validyne pressure

transducer.

After passing through the orifice, the water is piped to the air injection component

assembly. Figure 9 shows the exploded view of the injection component assembly. The

injection component assembly consists of three major parts: the water injection flange (#17),

the air injection nozzle (#15), and the top flange that houses the air nozzle (#16). The water

injection flange is the location where the auxiliary water (when used) was injected to generate

swirl in the water within the riser.
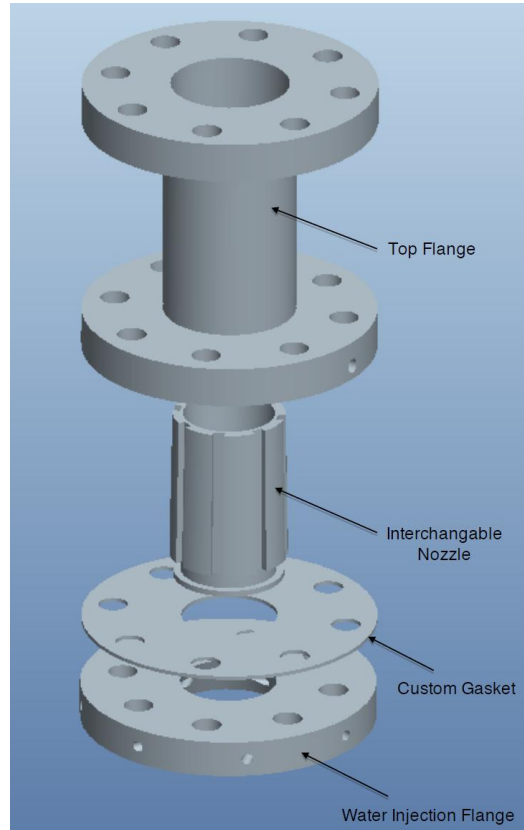
Figure 9: Exploded view of the injection component assembly.

The auxiliary water piping system is coupled to the primary water delivery system. A sump pump was placed in the tank, shown at the top of the system diagram in Figure 8. Water entering the pump is driven through 1-1/2" PVC tubing (#9), followed by a rotameter (#11), and then into a manifold (#12) with eight, equally spaced, outlets. Each outlet of the manifold was connected to the tapped inlets of the water injection flange, and through the flange to the tangential injection ports, seen in Figure 11. The hose taps of the manifold were connected to the hose taps on the water injection flange using clear, 30 psig, flexible PVC tubing with an inner diameter of 1/2". The length of each connecting piece of PVC, flexible tubing was 2-1/2" in order to ensure that the velocity of water flowing through each tangential injection port is equal in magnitude. Two valves, including a gate valve (#3) at the top of the system and a ball valve

(#10) at the bottom of the system, were used to regulate the flow rate being driven by the pump and to allow for the piping to be drained after operation was completed.

Figure 10 shows the two separate nozzles that were used during testing. Red arrows in the figure denote the path of air flow while the black arrows denote the path of the pumped water. The first nozzle, with nine helical spirals at an angle of 35° from the vertical axis, injects air with both axial and tangential velocity components. The second nozzle injects air in through eight vertical channels with only an axial velocity. Each interchangeable nozzle is tapered on the outside and fits into the bottom of the top flange piece. Air is injected into the top flange from a single, 5/8" threaded hole and flows into the bottom cavity of the nozzle before it enters the channels. See Appendix C for dimensioned drawings of major parts.
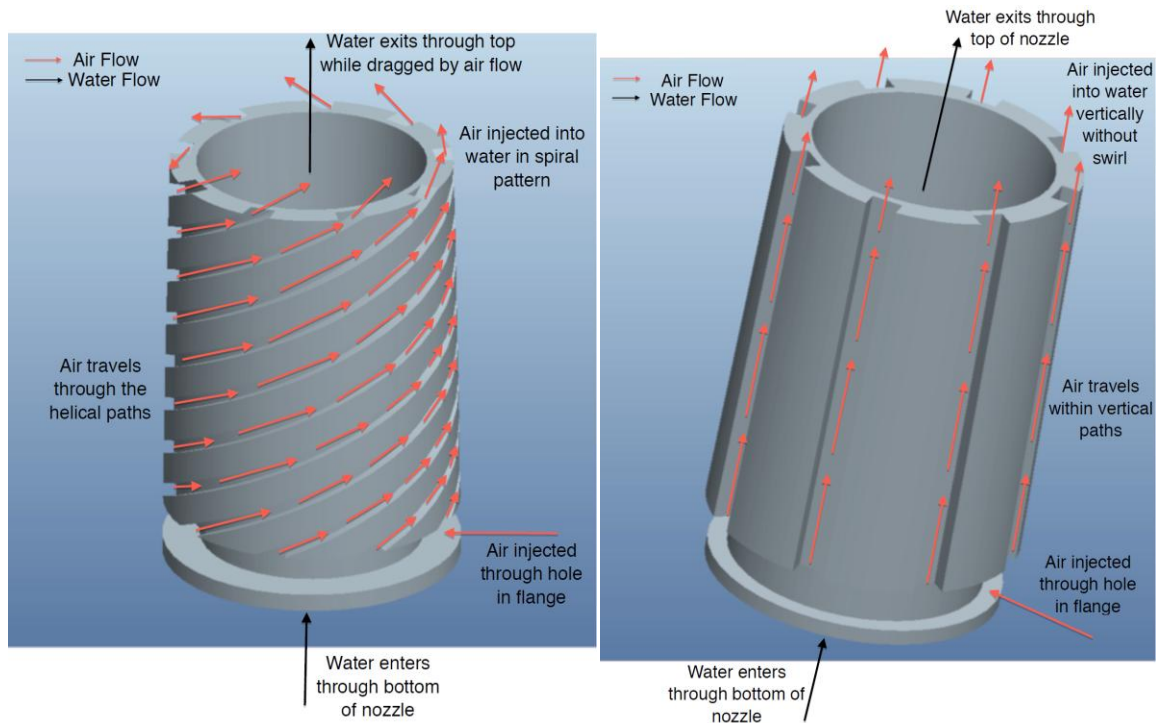
Figure 10: Water and air flow patterns through airlift pump and nozzle.

The water injection flange, shown in Figure 11, was manufactured from PVC and has holes drilled tangentially to the inside diameter. The red arrow shows the primary flow of water that is being fed through the piping. The black arrows show the water flow being injected by the sump pump. Water flows through the channels to drive a vortex flow on the inside surface, in the riser before the air injection point. A hose tap was inserted into each inlet, allowing the water injection flange to be connected to the manifold to receive the auxiliary water flow from the sump pump.

To be sure the current system behavior is consistent with previous experiments; the airlift pump was initially operated without the auxiliary water flow for the generation of riser swirl prior to air injection. The performance of the system was established by generating a graph showing water flow rate as a function of air flow rate, which was then compared to Finio's (2007) results. Data taken without the tangentially injected auxiliary water flow is expected to qualitatively agree with the corresponding data from Finio (2007). Quantitative differences in the data was to be expected since the experimental setups were not identical, having different inlet losses and different submergence ratios.
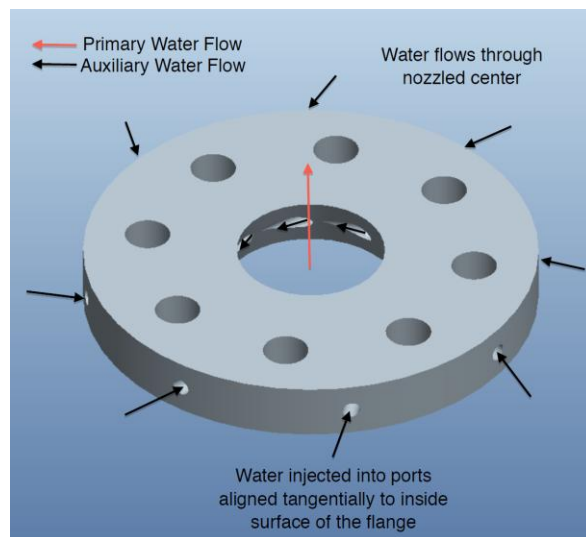
Figure 11: Water injection flange with both primary and auxiliary water flow.

Results and Discussion

Induced water flow rate measurements, taken with and without a tangential component in the air injection velocity, permit a direct comparison of pump performance with swirled air flow versus that with axial air flow. Similarly, induced water flow rates with and without the auxiliary tangential water flow injection permit an assessment of utility of this method of swirl generation.

Spiral versus straight air nozzles

Preliminary data was recorded to compare the current system with that used by Finio (2007). Figure 12 shows the induced water flow rate dependence on the input air flow rate for the spiral air nozzle. The water flow rates are substantially larger than the corresponding values found in Finio (2007), differing approximately by a factor of five. The increase in water flow rates in the new system relative to those of Finio is believed to be due to the reduction in losses in the pump inflow plumbing between the tank and the air injection point. In the current system there are significantly fewer sources of loss, since there are fewer elbows, contractions and expansions in the piping.

To generate added losses and check the hypothesized source of flow rate differences, the 4" valve located at the bottom of the system (#8 from Figure 8), shown in Figure 9, was closed to an angle of 75° from the fully open position. Closing the valve increased the minor losses of the piping system, which can be equated to an additional length of piping in the system. As the valve was closed, the loss coefficient of the valve (K-value) increased and approached infinity. With the valve closed to the 75° angle, the resulting water flow rates are closer to the data taken by Finio, as shown in Figure 13. The submergence ratio was kept constant at a value of 0.873 for all measurements in the

present system, while Finio's submergence ratio was approximately 0.591. The difference in submergence ratios is significant because the submergence ratio strongly affects the discharge flow from the pump, as was previously discussed in conjunction with Figure 2.
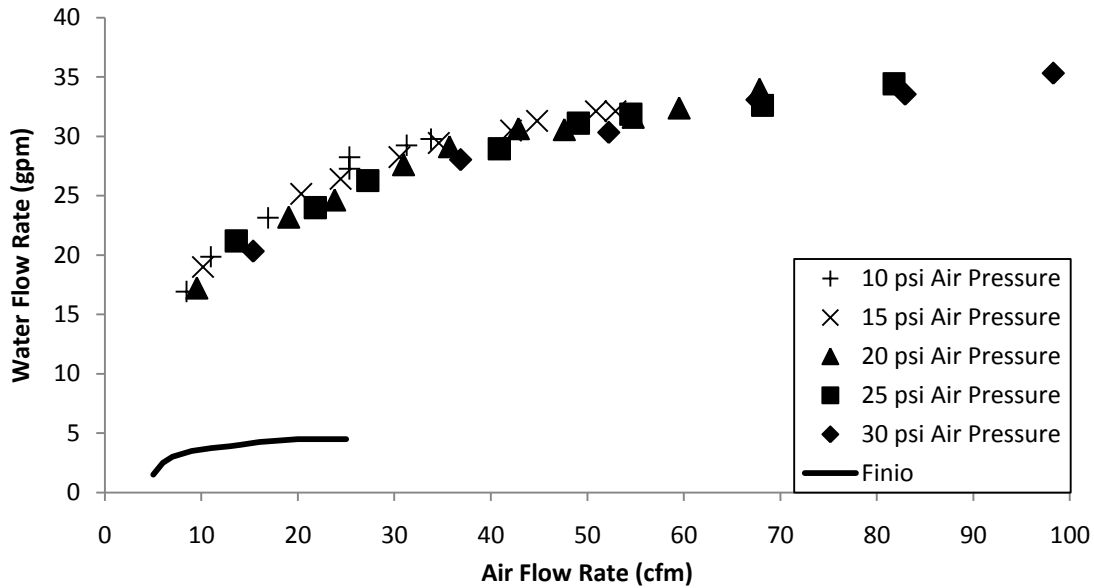
Figure 12: Induced water flow rate dependence on input air flow rate for various inlet air pressures, using the spiral nozzle.
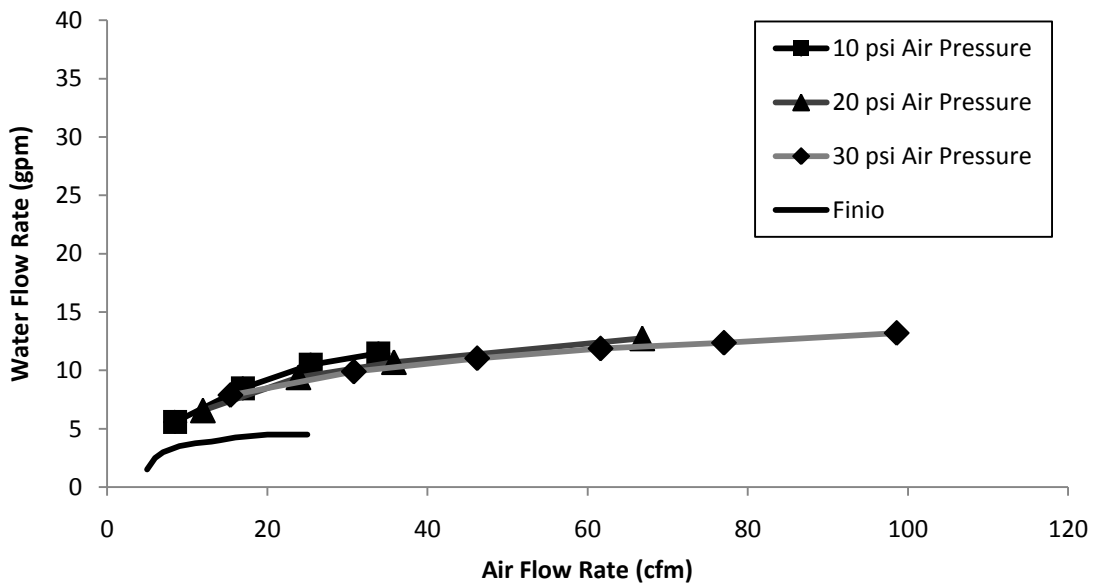
Figure 13: Induced water flow rate dependence on input air flow rate for inlet air pressures of 10 psig, 20 psig, and 30 psig using the spiral nozzle with the 4" valve at 75°. Lines included for visual clarity.

Water flow rates were measured using input air pressures of 10, 20 and 30 psig, for air flow rates from 5 scfm to a maximum value. The maximum possible air flow that could be measured with the array of measured pressures was 35 scfm. Figure 14 shows water flow rates obtained using the spiral nozzle for a variety of pressures, and valve openings as a function of the air flow rate. Figure 15 shows corresponding data sets obtained using the straight nozzle. The data in both Figures 14 and Figure 15, show that as the 4" nozzle is closed, the water flow decreases, due to larger minor losses. This decreasing flow rate with increased approach flow resistances is consistent with pipe flow behavior with increasing minor losses values due to valve closure.

In both Figures 14 and 15 for small air flow rates, the lower inlet air pressure (10 psig) yielded the highest flow rates of water compared to the higher pressures (20 and 30 psig). The higher water flow rates attainable with lower air pressures indicate that operating at lower air pressures is more efficient that operating at higher air pressures, since less work is required to compress the air to a lower pressure than that needed for a higher pressure. The trade-off of operating at lower pressure is that large air flow rates are unachievable from a single source. In Figure 14 and Figure 15, the maximum flow rate of the air that is obtainable at 10 psig is approximately 35 cubic feet per minute (cfm). The maximum water flow capacity of the pump can be achieved only with higher air flow rates, which are obtained at higher air inlet pressures. Figures 14 and 15 do not include the data at a valve angle of 0° since the data is almost identical to the data collected for a valve angle of 45°. Figure 16 shows the relationship between the efficiency of the system (the ratio of water mass flow to air mass flow) as a function of air flow. It can be seen that at lower air flows, the ratio between the two flows is much

larger than at significantly larger air flows. Figure 16 also compares efficiencies of both the spiral and straight nozzles. The hollow points represent the spiral nozzle. The only difference that can be seen between the two different nozzles occurs at lower air flow rates. At higher air flow rates, both nozzles yield approximately the same results. Therefore, since both nozzles yield approximately the same efficiency at all points of anticipated operation, the straight nozzle should be used during pump operation since it is simpler and easier to manufacture.
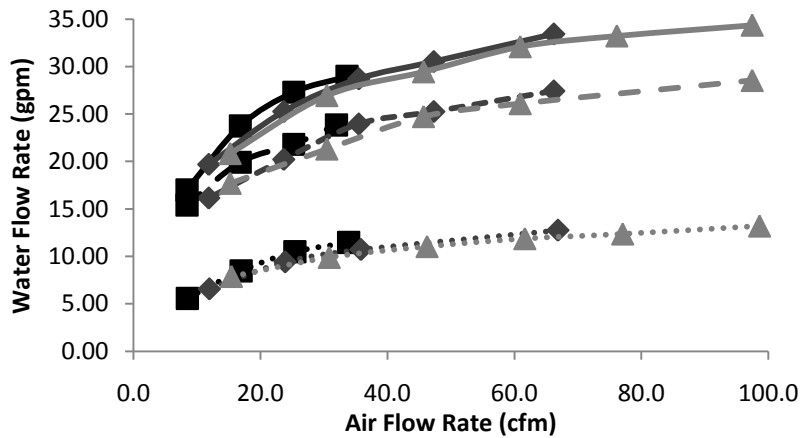
Figure 14: Pump performance comparison for 4" valve settings of 45°, 60° and 75° degrees at 10, 20, and 30 psig air pressures, *using the spiral nozzle*. Solid, dashed, and dotted lines represent valve settings of 45°, 60° and 75° and square, diamond, and triangle points represent 10, 20, and 30 psig. Lines are included for visual clarity.
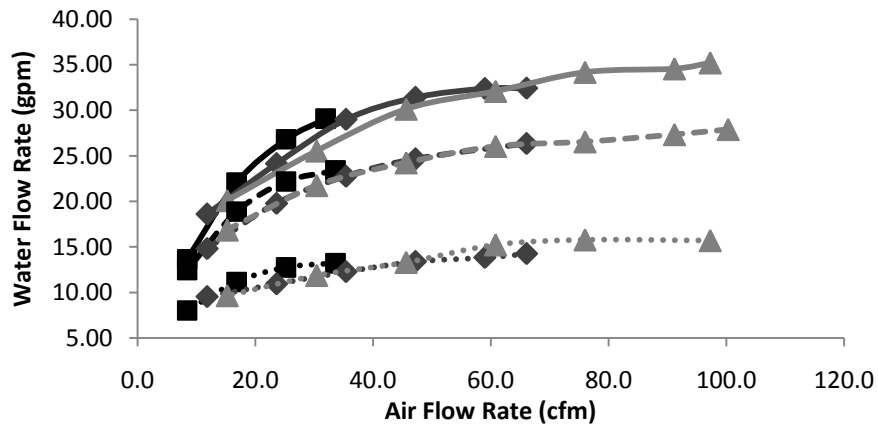
Figure 15: Pump performance comparison for 4" valve settings of 45° 60° and 75° at 10, 20, and 30 psig input air pressure, *using the straight nozzle*. Solid, dashed, and dotted lines represent valve settings of 45°, 60° and 75° and square, diamond, and triangle points represent 10, 20, and 30 psig. Lines are included for visual clarity.
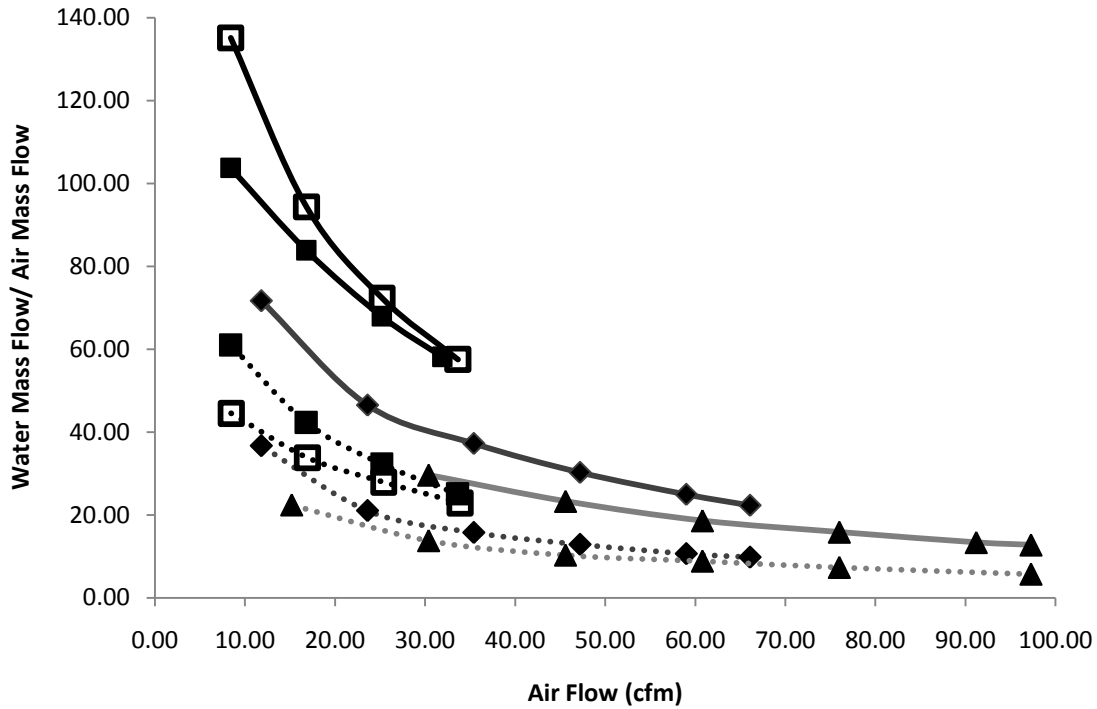
Figure 16: Relationship between water-air mass flow ratio and injected airflow. The straight nozzle is represented by solid points while the spiral nozzle is represented by the hollow points. Solid, dashed, and dotted lines represent valve settings of 45°, 60° and 75° and square, diamond, and triangle points represent 10, 20, and 30 psig. Lines are included for visual clarity.

Figures 17 and 18 provide direct comparisons of airlift pump performance with the spiral nozzle to that obtained with the straight nozzle for air inlet pressures of 30 psig and 10 psig, respectively. Figures 17 and 18 were generated using the same data that was used in Figures 14 and 15 with the data taken from the spiral and straight nozzles compared while keeping pressure constant. In both Figures 17 and 18 with the 4" valve set at 75°, the straight nozzle yielded a water flow rate approximately 2.5 gpm greater than that for the spiral nozzle operating with the same air flow rate. In Figure 17 (for 30 psig air injection pressure with the 4" valve at 45° and 60°), there is no noticeable difference in the water flow rates with the spiral and the straight nozzles. In contrast, with 10 psig inlet pressure, the spiral nozzle performed better than the straight nozzle at

the lower air flow rates with the 4" valve set at 45° and 60°, as shown in Figure 18. For

air flow rates greater than 20 cfm, the two nozzles yield similar water flow rates with the

valve at 60°. With the valve at 45°, the spiral nozzle produces decreasingly better water

flow rates with increasing airflow rates until a flow rate of about 28 cfm, after which the

two nozzles yield almost the same water flow rate. Trends between the results seen in

Figure 16 are similar to the trends seen in Figures 17 and 18.
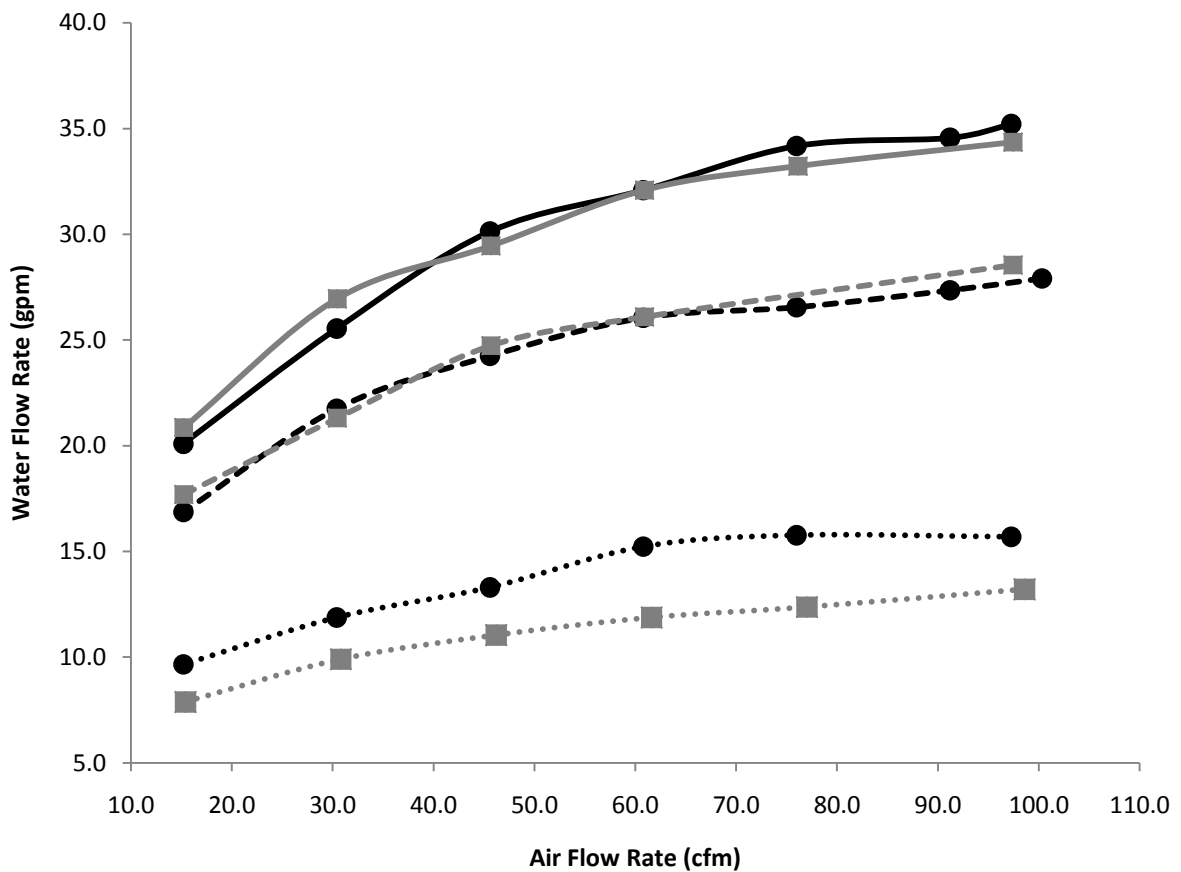
Figure 17: Airlift pump performance comparison for spiral and straight nozzles with an
air input pressure of 30 psig. Solid, dashed, and dotted lines represent valve settings of
45°, 60° and 75° and square and circle points represent the spiral and straight nozzles.
Lines are included for visual clarity.

Figure 18: Airlift pump performance comparison for spiral and straight nozzles with an air input pressure of 10 psig. Solid, dashed, and dotted lines represent valve settings of 45°, 60° and 75° and square and circle points represent the spiral and straight nozzles. Lines are included for visual clarity.

Swirl induced by auxiliary tangential water injection

Figure 19 shows the net pump water flow when the auxiliary water flow was injected through the swirl flange with the spiral nozzle. During initial testing, with the 4" valve closed the sump was operated at full capacity and the maximum measured auxiliary water flow rate was found to be approximately 17 gpm.

With the 4" valve open at a selected angle (60° or 75°), pump performance in terms of net water flow rate was measured. These measurements were taken using an air flow of 20 scfm at 20 psig air pressure (airflow of 47.7 cfm after taking air temperature

and atmospheric pressure into account). The procedure for calculating airflow in cfm is shown in Appendix D. As the auxiliary water flow rate increased, the pump performance decreased approximately equal to the flow that was induced using the auxiliary water flow. It was anticipated that the swirl induced by the auxiliary water injection would create a low pressure at the center of the pipe with a high pressure around the periphery inside the pipe, resulting in an increase in flow as air was introduced to the system. The tangential water injection did create a low pressure at the center, but only a fraction of the injected water mass flow was drawn up the riser. A substantial portion of the auxiliary water flow flowed back through the piping diminishing the net water flow rate being drawn from the tank. The backflow caused by the increased pressure at the pipe periphery is caused by two major factors. The first factor is that the injected water is the same density as the water already being driven in the primary water flow system. Since there is no difference in density, no buoyancy effects are present between the primary water flow and the auxiliary water flow. It would be desirable to have the auxiliary water flow to have a slightly lower density in order to help drive the primary water flow, while still being able to have a density large enough to produce a more effective momentum transfer between the primary and auxiliary water flows. In Figure 20, the normalized net water flow as a function of the auxiliary water flow for the straight nozzle is shown. The flow is normalized using the water flow rate generated by the air input when the no auxiliary water flow is delivered to the system. At any value of auxiliary water flow, if the normalized net water flow is greater than one, the swirling of the water will be beneficial to pump performance. If the value is below one, the swirl is detrimental to pump performance and operation without the swirl would yield a higher output.

Performance degradation is seen in both Figure 19 and 20. All recorded data can be found in Appendix E.
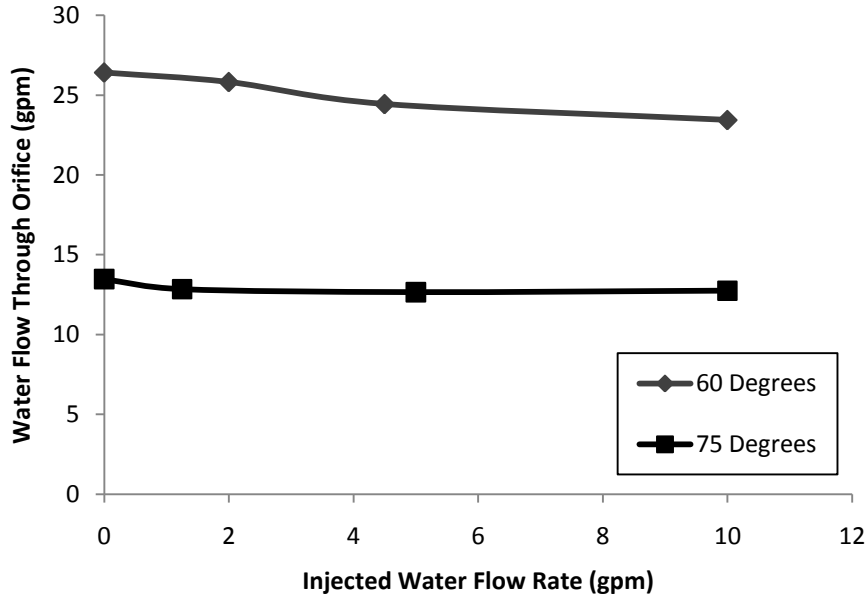
Figure 19: Water flow rate behavior with increasing auxiliary water flow with the 4" valve at 60° and 75°, using the *spiral nozzle*. Lines are included for visual clarity.
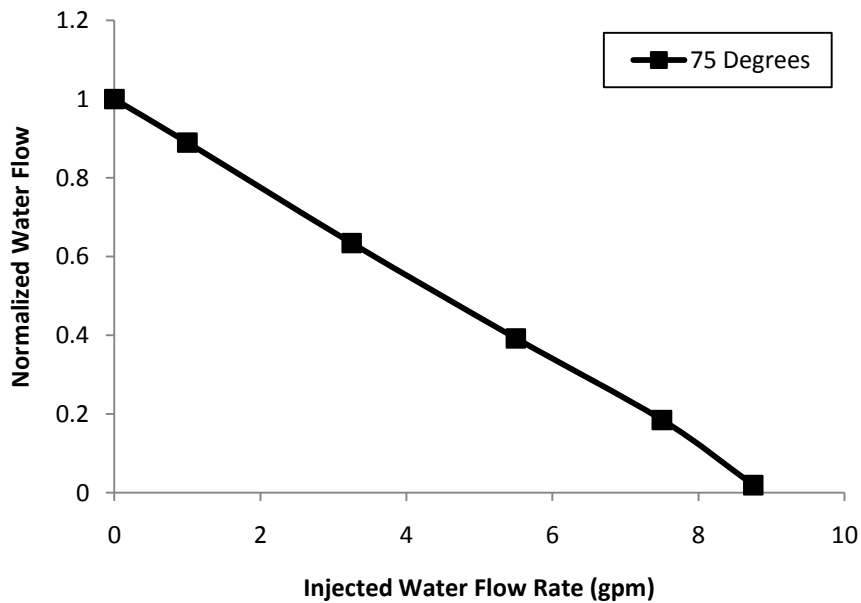
Figure 20: Normalized net pump flow rate behavior with increasing auxiliary water flow with the 4" valve at 75°, *using the straight nozzle*. Lines are included for visual clarity.

A theoretical analysis was undertaken to determine the extent of backflow occurring in the current system and to determine the head required to drive the auxiliary flow entirely up the riser without backflow. The backflow of the auxiliary water flow occurs because less head is required to drive the flow backward through the system to the tank than to drive the flow up the riser. Water flows through the path of least resistance. In order for the water to flow purely up the riser, the backflow head loss needs to be increased until it is greater than the head required to drive the auxiliary flow vertically up the riser. Closing the 4" valve can increase the backflow head. The minor losses and the backflow loss head increase as the valve is closed.

Figure 21 shows the loss coefficient (K-values) obtained by Blevins (1984) plotted as a function of valve angle away from the open position (0°). An empirical, best fit, exponential curve was fit to the experimental data is shown in Figure 21. Using the empirical curve fit, loss coefficient values were extrapolated for the valve angles of 60° and 75° that are not available from experimental data. The head curves for both backflow head loss and lift head as a function of water flow rate from the auxiliary system at each valve position are given in Figure 22. During auxiliary water flow, pure lift may only be achieved when the 4" ball valve position is at 75°. Since an exponential fit was used for the available data in Figure 21, large errors could easily be incurred in extrapolating the curve fit at larger valve angles. Figure 22 shows that the backflow head and the lift head are equal at approximately 10 gpm. The actual point where the flow is equal for a 75° valve angle is within a few gallons per minute of the value shown on the graph. Theoretically, as the auxiliary water flow exceeds the water flow yielding equal values

for both backflow head loss and regular lift head, the swirl component will begin to produce positive effects.
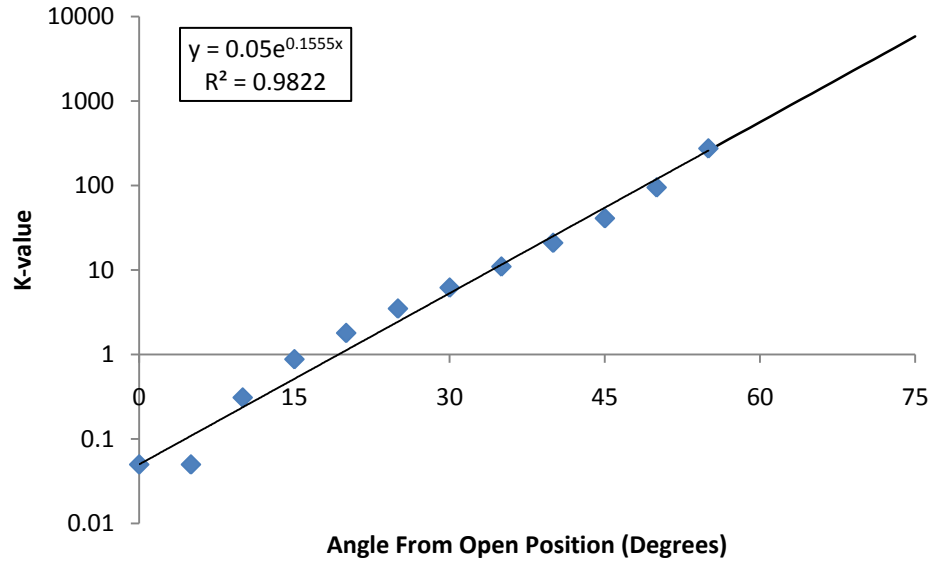
Figure 21: Experimental loss coefficients dependence on the position of the valve from the open position for the 4" ball valve. Data points from Blevins (1984).
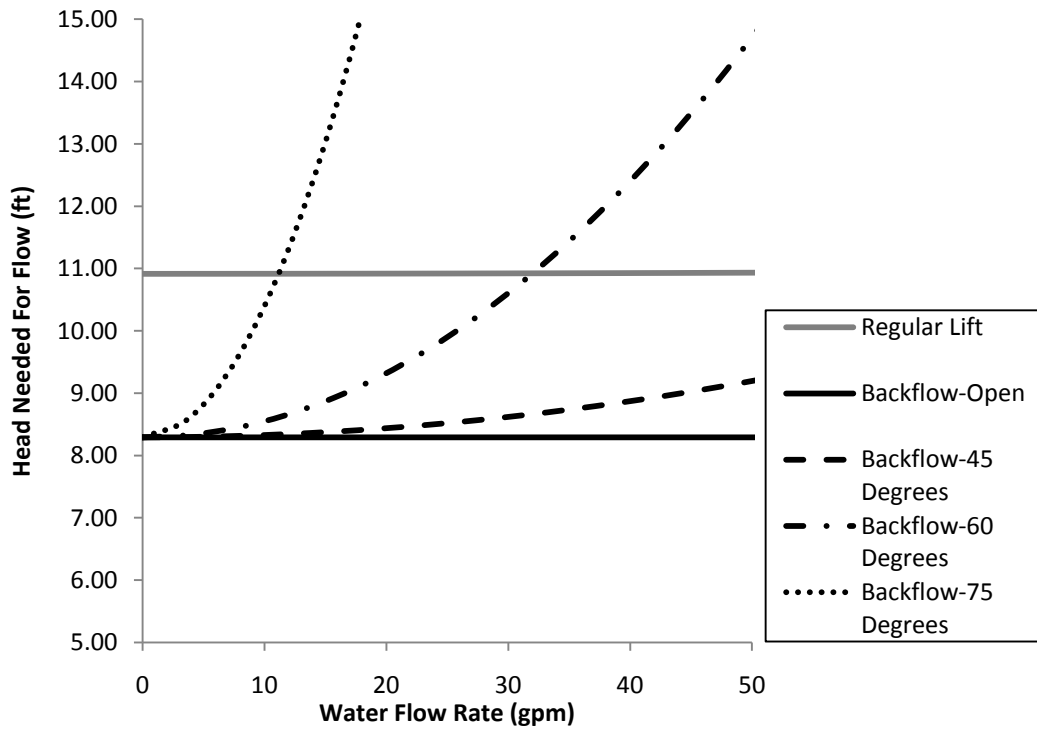
Figure 22: Head required for flow for a given auxiliary water flow with the current experimental setup.

Even if the auxiliary swirl flange was repositioned from its current position to a location further up the riser where it was level with the free surface of water in the tank, sufficient regular lift would only occur at or beyond maximum auxiliary water flow rate, as shown in Figure 23. The idea is that elevating the auxiliary injection flange to a point up the riser, less backflow would occur because less head would be required for flow to travel up the riser (regular lift). However, from Figure 23, simply elevating the swirl flange, alone, does not increase pump performance. Figure 23 shows head characteristics similar to that of Figure 24, and therefore elevating the auxiliary water flange will not eliminate the backflow and the desired flow through the orifice will still be resisted by a portion of the injected auxiliary water flow. Figure 24 shows an analysis using the same riser lift used in Figure 22, assuming the system is a vertical pipe with a known submergence, S. For each depth of submergence, a value of auxiliary water flow is determined for the point where the induced swirl begins to yield an increase in performance. Using the current sump pump at maximum capacity, a pipe with a submergence of approximately 500 feet below the free surface would be needed before any positive performance would be observed. When the sump pump operates at maximum capacity (approximately 16 gpm), in order for pump performance to be beneficial, the backflow head must be greater than the head required to lift the fluid up the riser. As seen in Figure 24, at a pipe length of 500 feet, the backflow head exceeds the regular lift head only when the auxiliary water flow rate is at approximately 14 gpm. Therefore, beneficial effects in pump performance would begin to be observed.
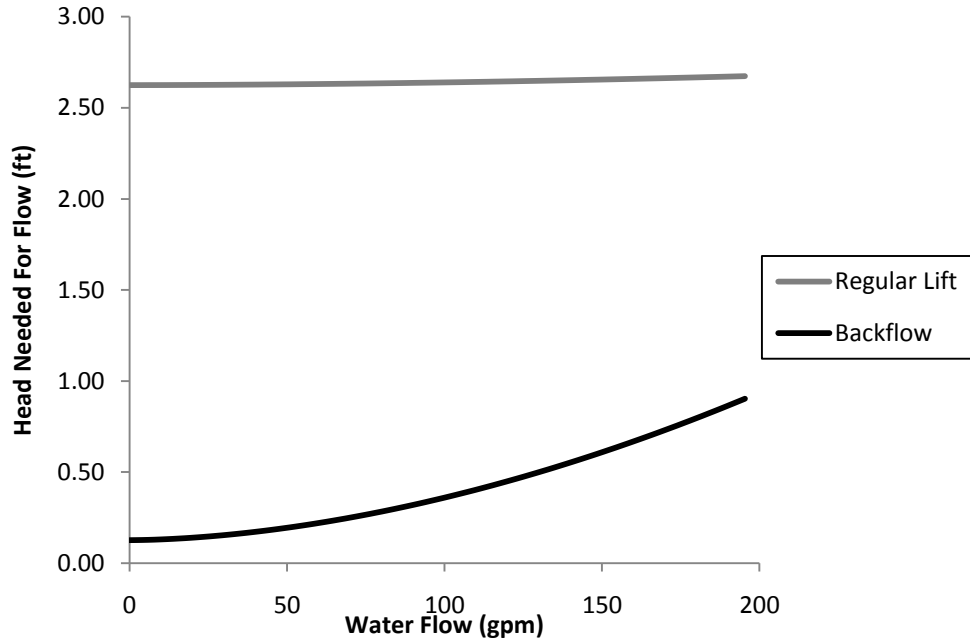
Figure 23: Head required for flow for a given auxilliary water flow for case when auxiliary water injection flange is repositioned to a location that is level with the tank water level.
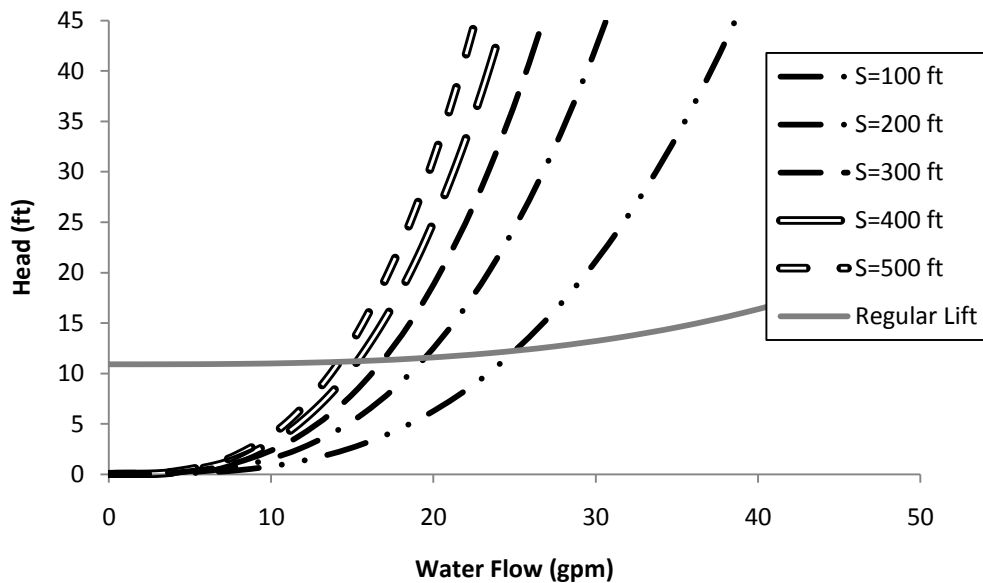
Figure 24: Required head for a given water flow for simple, submerged pipe with a lift of 10.92 ft where S is the submergence.

Since it was determined that positive effects in pump performance should be observed at maximum capacity of the auxiliary water flow, the airlift pump was operated to determine if the results from the theoretical analysis matched experimental

29

observations. The swirl component did not produce any positive changes in performance when the auxiliary water flow was operating at full capacity, despite the water flow exceeding the theoretical point where the swirl would produce a positive effect. At higher flows from the swirl component, the air became entrained in the center, low pressure, portion of the pipe. The multiphase flow occurring at the higher auxiliary water flow rates resembled the annular flow regime. The only difference is that the water annulus surrounding the air had radial accelerations and axial accelerations as opposed to purely axial accelerations. When the air flows through the center of the pipe, water flow is driven only by the shear force resulting from the interaction between the water and air. A large slip ratio exists between water and air, causing the flow to be inefficient. Ideally, water is driven by air flow with a large surface area of bubbles with the resulting buoyant and drag forces driving the water flow up the piping (slug flow regime). Operating the swirl at high auxiliary flow rates is not conducive to creating the conditions needed for maximum and efficient water flow to occur in the system.

During airlift pump operation, depending on valve settings, the system may have a wide range of losses. The major and minor losses can be used to generate an equivalent length that treats all losses as a length of piping experiencing the effects of friction. The equivalent length simulates the pipe length beneath the air injection point that would be needed to produce losses equivalent to those from the system with valves, elbows, contractions, etc. The analysis formulating an equivalent length allows for the piping system to be analyzed easier with one variable (the equivalent length) as opposed to multiple variables in the system setup (bends, contractions, and other losses). The

relation used to determine equivalent length is Equation 1.

$$f\left(\frac{L_{eq}}{D}\right)\left(\frac{1}{2}\rho V^2\right) = \left[f\left(\frac{L_{actul}}{D}\right) + \sum K\right]\left(\frac{1}{2}\rho V^2\right) \tag{1}$$

where:

f is the friction factor,

L_{eq} is the equivalent length of pipe, in feet,

D is the diameter of the piping, in feet,

K is the K-value of the minor losses within the system,

L_{actual} is actual length of piping before the point of air injection, in feet,

ρ is the density of the fluid, in lb-mass per cubic feet,

and V is the velocity of the fluid, in feet per second.

The right side of Equation 1 shows the head loss from both minor losses and major

losses. Equation 1 simplifies to the Equation 2. The ratio between the equivalent pipe

length and pipe diameter is obtained.

$$\frac{L_{eq}}{D} = \frac{L_{actual}}{D} + \frac{\sum K}{f} \tag{2}$$

Figures 25 and 26 show the relationship between the water flow and the ratio between the

calculated equivalent pipe length and the pipe diameter for the straight nozzle and spiral

nozzle. Data points were taken from the data acquired during testing. The ratio of

equivalent length to pipe diameter was determined by using the loss coefficient for the 4"

valve along with the rest of the loss coefficients in the system. The resulting ratios of

equivalent pipe length to pipe diameter was then matched to the corresponding water

flow rate at each setting. For both Figures, air flow was held to a range of 23-25 cfm.

Although the air flow is not constant, its deviation from a constant value is small enough

31

to assume it is approximately constant. At low valve angles, a smaller K-value (minor losses) will be present and flow is not choked significantly. Smaller K-values yield a shorter equivalent length of pipe. When the valve is open, or close to the open position, a there will be a small K-value for that setting. Due to the exponential relationship between the K-values and the valve angle, an exponential trend will be seen as the valve setting approaches 90° (closed position). As the valve is closed the minor losses increase exponentially, resulting in the equivalent pipe length increasing monotonically and the water flow slowed considerably. Figures 25 and 26 verify the relationship between air inlet pressures seen in Figures 13-16. The relationship between the efficiency and the ratio of equivalent pipe length to pipe diameter is seen in Figure 27. As the equivalent pipe length increases, the efficiency of the system decreases.
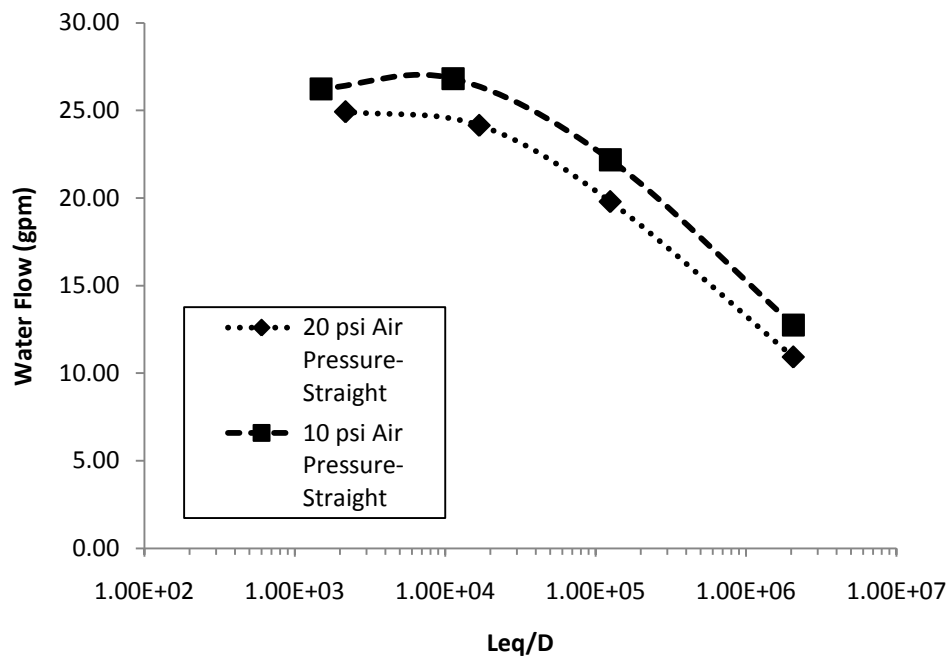
Figure 25: Water flow as a function of L_{eq}/D for the straight nozzle. Air flow was approximately constant in the range from 23 cfm to 25 cfm. Lines are included for visual clarity.
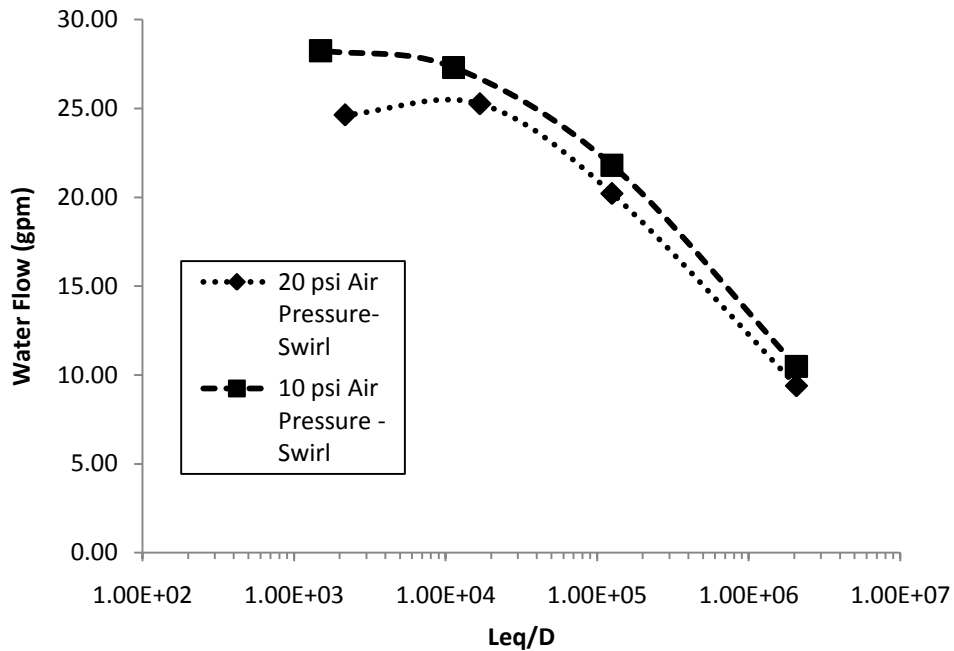
Figure 26: Water flow as a function of L_{eq}/D for the spiral nozzle. Air flow was approximately constant in the range from 23 cfm to 25 cfm. Lines are included for visual clarity.
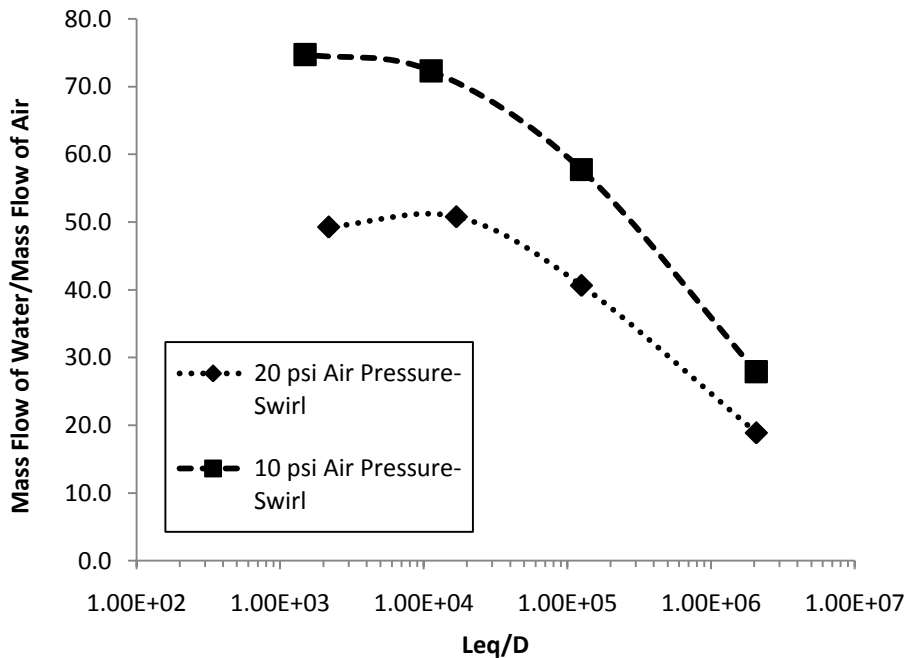
Figure 27: Water mass delivered per unit air mass input as a function of L_{eq}/D for the straight nozzle. Air flow was approximately constant in the range from 23 cfm to 25 cfm. Lines are included for visual clarity.

Conclusions

       The results of the experiments showed that swirling the airflow has only limited beneficial effects on the performance of the pump. Both nozzles delivered approximately the same water discharge for the same air injection flow rates (except for the lowest flow rates) at the same injection pressures. The spiral nozzle did deliver slightly greater water flow rates for the lowest range of air flow rates tested. These low injection air flow rates would seldom be used in practice since they do not provide a sufficient water flow rate for most industrial applications. The cost and time required to produce the swirl nozzle far exceeds that of the straight nozzle. The straight nozzle is recommended for pump operation due to the relative ease of manufacturing.

       During airlift pump operation with the present configuration, it is recommended that the air inlet pressure be set to approximately 10 to 15 psig (this value will need to be adjusted based on the submergence of the injection point and system setup). Results from testing showed that low air pressures yield water flows that are approximately 80% of the maximum attainable water flow for the system while operating with a higher efficiency. The higher efficiency for operating at 10 psig is due to the fact that less power is required to compress atmospheric air to 10 psig than to compress air at the same atmospheric conditions to 30 psig.

       Additionally, it was discovered that the addition of auxiliary water flow tangential injection to generate riser swirl was detrimental to the performance of the airlift pump. As the swirl was introduced, a substantial portion of the auxiliary water flow was driven back through the piping and produced added resistance to the desired, primary water flow. It was determined that the only way for swirl to benefit pump performance was to

have a large piping losses or an extremely long length of pipe in the system beneath the

air injection point to provide sufficient resistance to backflow. At high auxiliary water

flow rates, the detrimental effects from the swirling riser flow are amplified as air is

driven to the center of the pipe, reducing the effective area of the air flow.

References:

Blevins, R. 1984 "Applied Fluid Dynamics Handbook," Van Nostrand Keinhold Company, Inc, pp. 88.

Clark, N.N. and Dabolt, R.J. 1986 A general design equation for air lift pumps operating in slug flow, **AICHE J. 32**, pp. 56-63.

Finio, B. 2007 *Performance Characteristics of a Vortexing Jet Pump,* Undergraduate Honors Thesis, Department of Mechanical Engineering, Bucknell University.

François O, Gilmore T, Pinto MJ, Gorelick SM. 1996 A physically based model for air-lift pump- ing, **Water Resources Research, 32,** pp. 2383–99.

Knisely, C.W. 2010 Personal Communication.

Knisely, C.W. & Finio, B. 2010 Experiments on Vortex-Driven Air-Lift Pumps, ISEM Conference, Kyoto, Japan Nov 4-8, 2010.

Pickert, F. 1932 The theory of the air-lift pump, **Engineering**, 134, pp. 19-20.

Stenning, A.H. and Martin, C.B. 1968 An analytical and experimental study of air-lift pump performance, **J. Eng. Power 90 (2)**, pp. 106-110.

Zenz, F.A., Explore the Potential of Air-Lift Pumps and Multiphase, **Chemical Engineering Progress**, August 1993, pp. 51-56.

Appendix A: Part List

The table shown below lists the parts used in the system (Figure 8)

Table A1

Part Number	Description	Manufacturer	Model Number
1	Large plastic water tank - approx. 5'x4'x3'	-	-
2	1/3 hp-6 Series, Sump Pump	Little Giant	6-CIM-R
3	1-1/2" True Union PVC Gate Valve	McMaster-Carr	46065K81
4	4" Schedule 40 PVC pipe	Harvel	1120
5	Pressure Transducer	Valydine	DP15-30
6	.7 ID Orifice Plate	-	-
7	Drain Valve	-	-
8	4" True Union PVC Ball Valve	Hayward	LB309
9	1-1/2" Schedule 40 PVC pipe	McMaster-Carr	48925K15
10	1-1/2" True Union PVC Ball Valve	Webstone	3826
11	Rotameter (for water)	Omega Engineering, Inc.	FL-73 Series
12	Custom Manifold	-	-
13	Rotameter (for air)	King Instrument Co.	7205-0161-A
14	1/2" air control valve	B&K/Mueller	-
15a	4" Interchangable Nozzle with 9 Helical Spirals	-	-
15b	4" Interchangable Nozzle with Vertical Channels	-	-
16	Top Flange	-	-
17	Water Injection Flange	-	-

Appendix B: Calibration

The Valydine pressure transducer was calibrated by reading the percent of maximum pressure that can be experienced across the film that was placed in the transducer, while measuring the water at the discharge of the system. At the system outlet, water is collected in a bucket over a given period of time. The water is weighed using as scale. The resulting weight, divided by the time period during water collection, yields the mass flow rate. Ten to fifteen samples were taken at air flow rates of 10 scfm, 20 scfm, and 35 scfm. (Subsequently, the scfm units were converted to cfm using measured atmospheric pressure and temperature) The square of the measured mass flow rate has a linear relationship with the pressure reading. Figure 1A shows the linear trend between the squared water mass flow and the pressure for the first calibration. A second calibration was done, with the linear trend seen in Figure 2A. The first calibration of the system was done using a scale that was only capable of measuring up to 11 pounds. Water would be pumped out at a rate to fill the bucket within one to two seconds. The short time period, coupled with the natural oscillations of the water flow discharge, resulted in significant error in the fitted trend. Due to this error, a second calibration was done to reduce the deviation between measured values and the average at each air flow rate. A new scale, capable of 150 lb loads, was used for the second calibration. The new scale allowed for the water to be collected until the bucket was almost filled. The time period of water collection for the second calibration was between three and four seconds. The second calibration yielded data that had significantly less deviation than that of the first calibration. The coefficient of determination (R^2) improved significantly from the first to the second calibration. The larger coefficient of determination seen in Figure 2A

indicates that the second calibration has a better fitted trend through the data. Figure 3A shows the calibration that was done after a new Valydine pressure measurement unit was acquired. The calibration curve from Figure 3A was used only for the investigation of swirling the water flow with the straight nozzle (Figure 21).
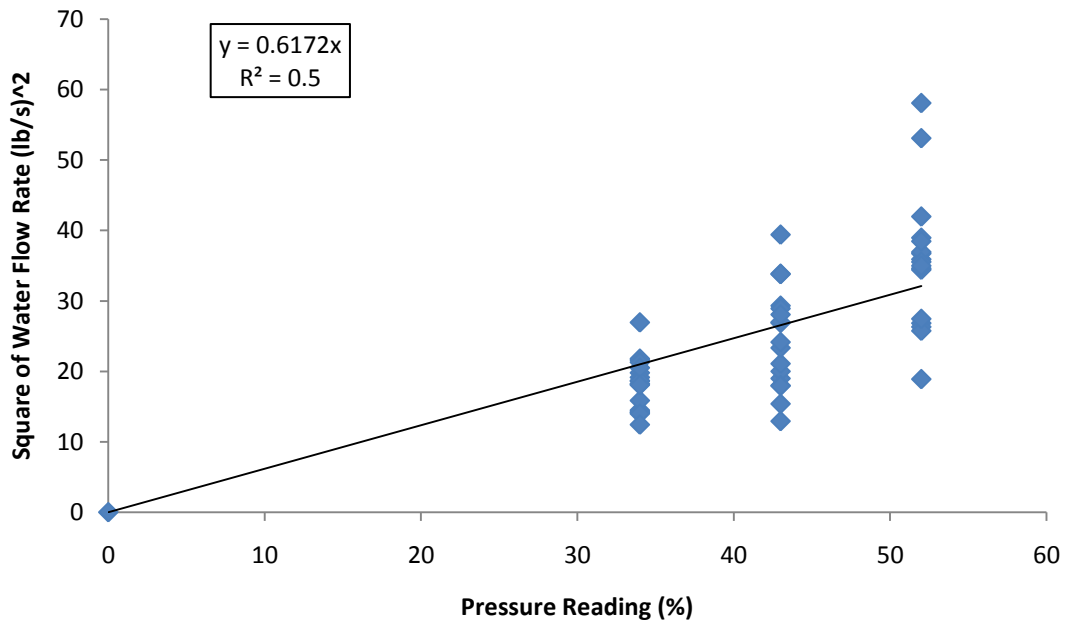
Figure 1A: Mass flow squared dependence on pressure reading.
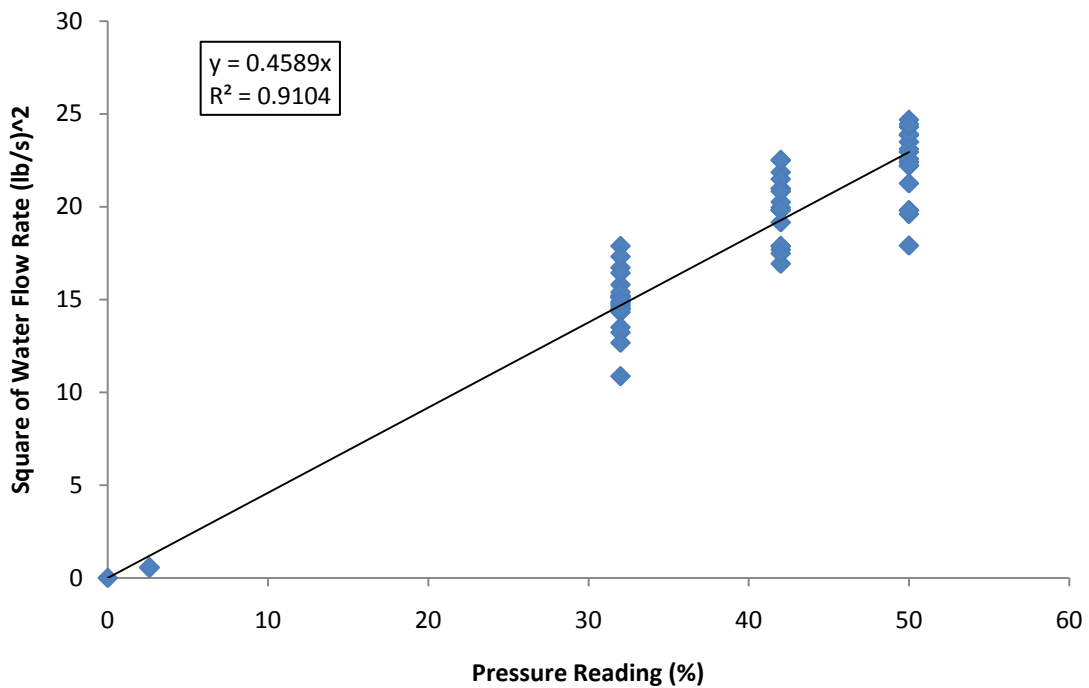
Figure 2A: Mass flow squared dependence on pressure reading.
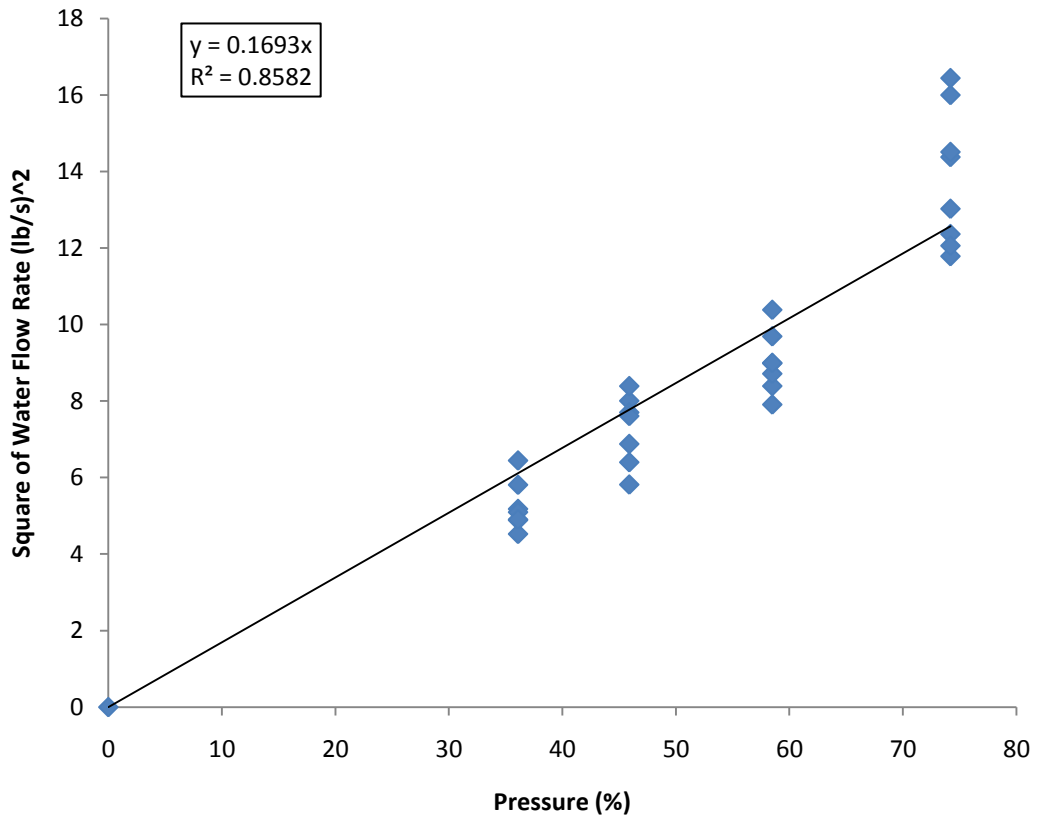
Figure 3A: Mass flow squared dependence on pressure reading.

Appendix C: Part Drawings

The following pages contain the drawings for relevant machined parts. The drawing for the helical nozzle does not have sufficient information for machining due to complicated parameters of the part. The sufficient ProE and CAD files for the production of the part can be found in the Bucknell University Library with thesis materials from the work done by Finio (2007).
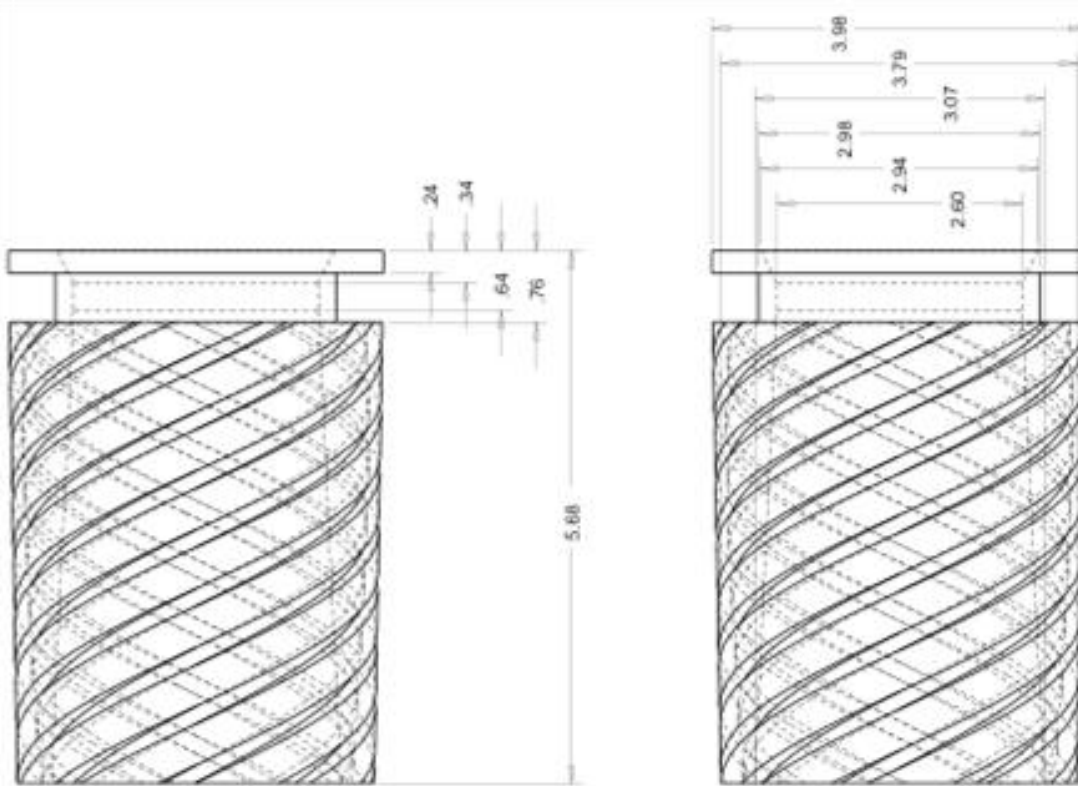
Nozzle with 9 helical spirals

All units in inches

Nozzle is tapered from base to top by 1°

.20

.58

.80

89.00°

6.00

2.00

1.88

1.63

1.61

1.55

1.25

.25

.40
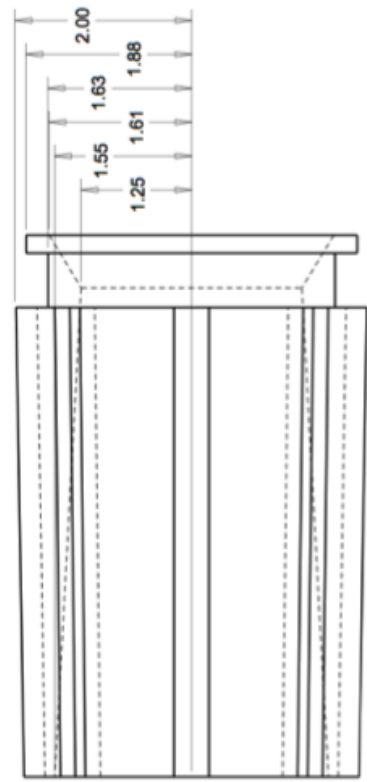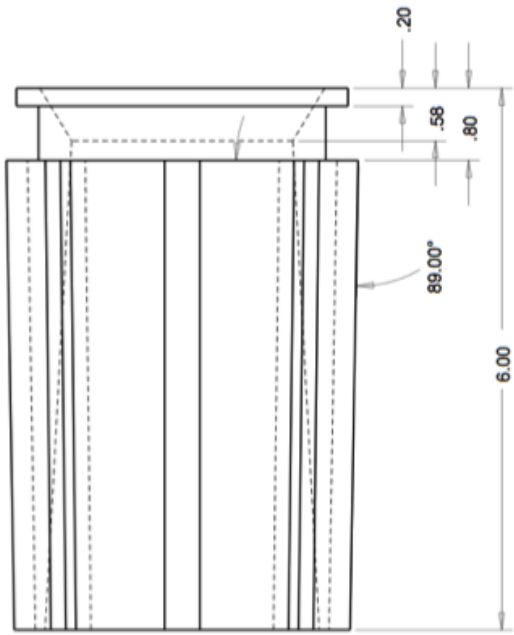
Channels placed at 45 degree angles about the central axis.
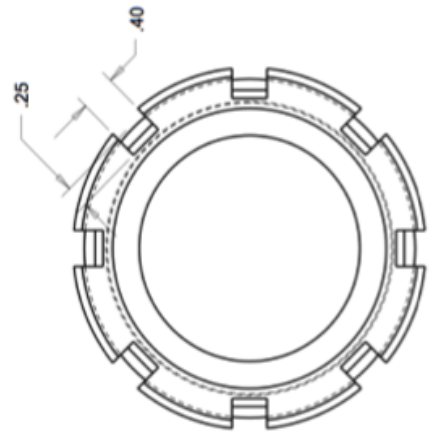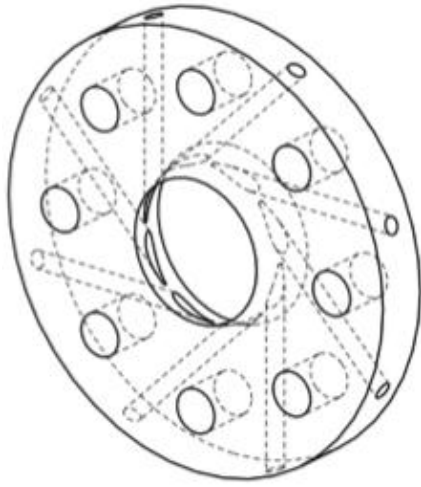
All units in inches.

Holes and channels both distributed in 45 degree increments about the central axis.

Channels are tangential to the inner surface of the flange.

R5
R2
R1-5/8

8X⌀3/8

8X⌀1

3-5/8

5/8

1-1/4

.13

45.0°

4.00

SCALE 1.000

8X⌀1.00

⌀10.00

⌀3.25

46
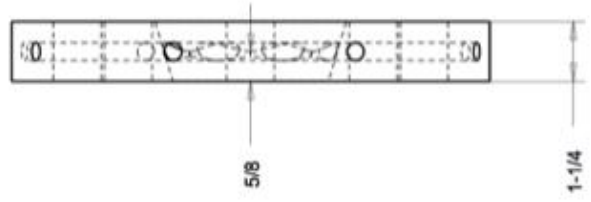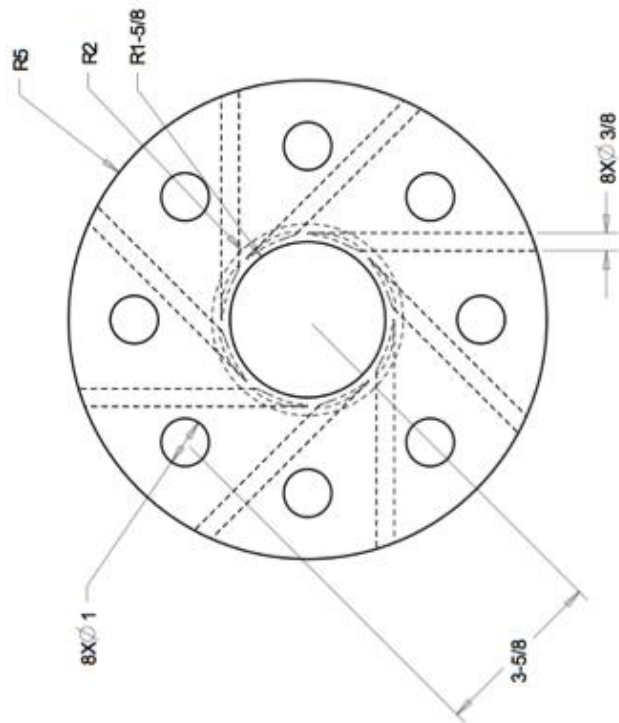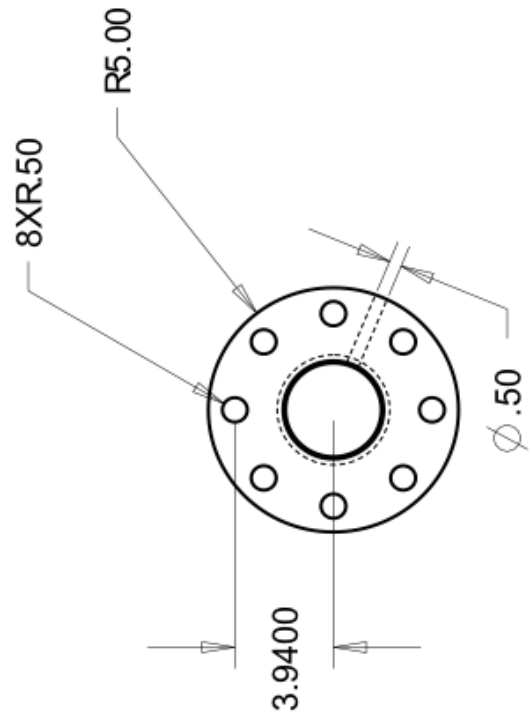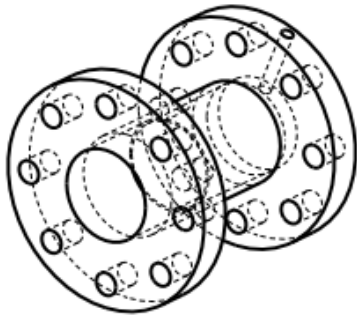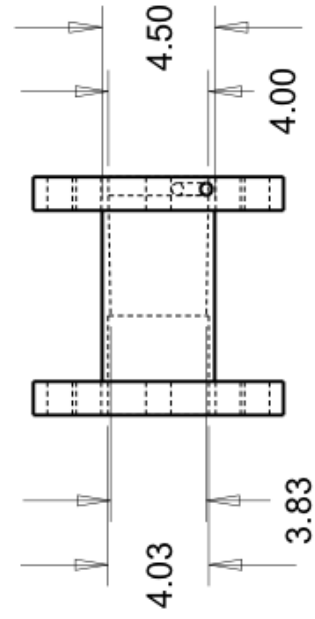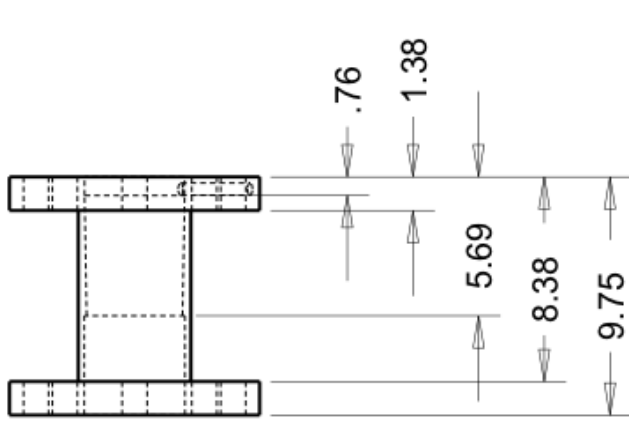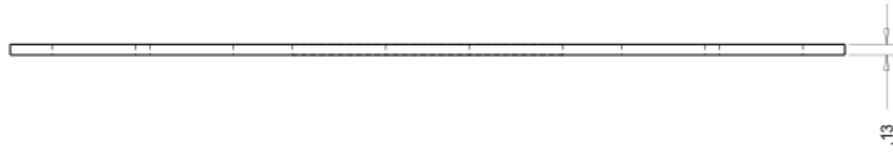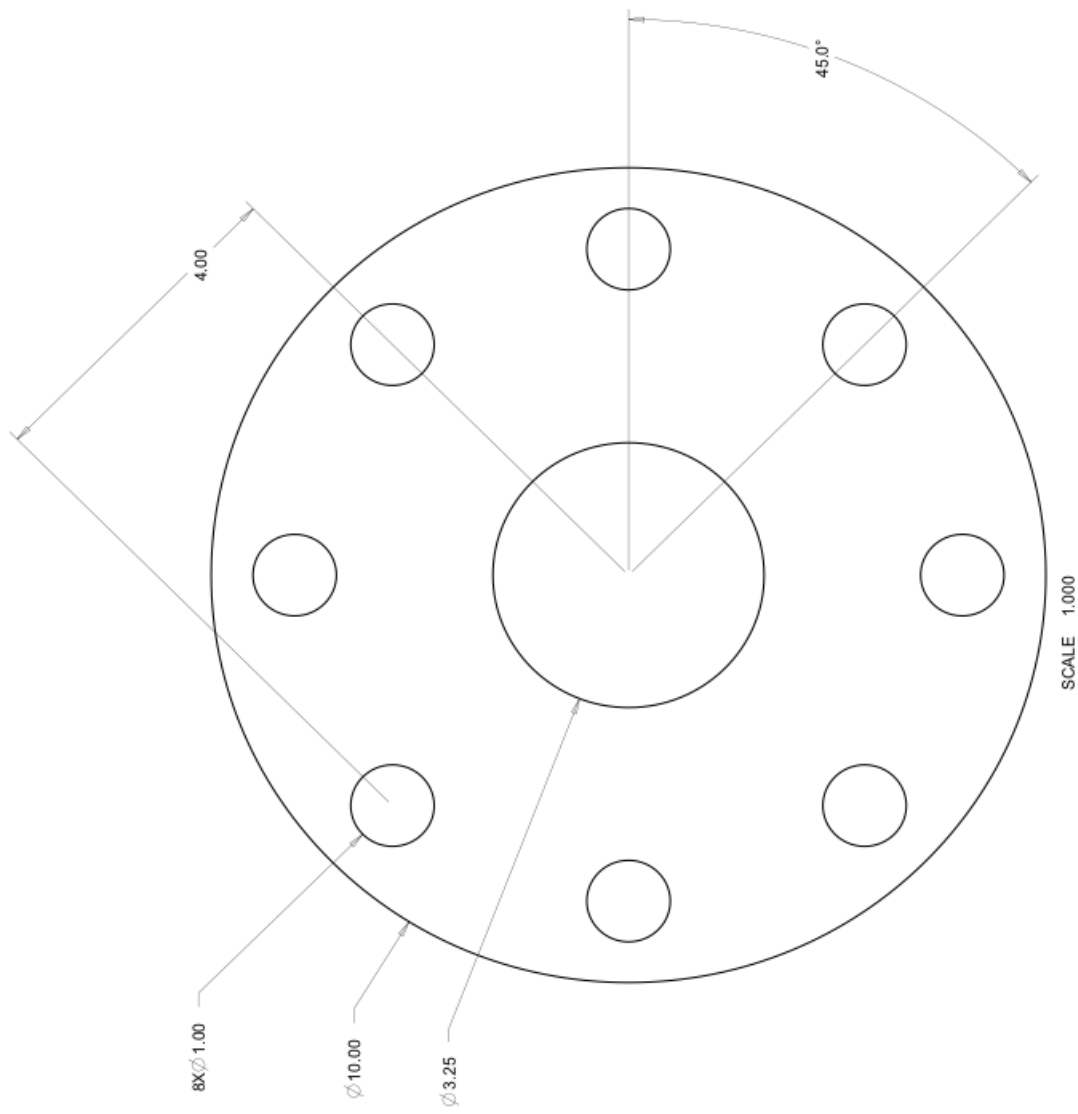
Appendix D: Air Flow Conversion

Air flow rates are measured from the rotameter (Part 13 in Table 1) have units of scfm.

The measured flow does not take the density of the injected air into account. In order to

obtain the value of air flow, the recorded air flow is multiplied by the ratio between the

density of the air that is injected at the air inlet and the density of the air at atmospheric

pressure:

$$\dot{Q}_{Air,cfm} = \dot{Q}_{Air,scfm} \left(\frac{\rho_{air,inlet}}{\rho_{air,atmospheric}} \right)$$

where:

$\dot{Q}_{Air,cfm}$ is the desired air flow rate at the inlet, in cfm,

$\dot{Q}_{Air,scfm}$ is the measured air flow rate at the inlet, in scfm,

$\rho_{air,inlet}$ is the density of the air at the inlet, in lbm/ft^3,

$\rho_{air,atmospheric}$ is the density of the air at atmospheric pressure, in lbm/ ft^3,

Appendix E: Data

Table 1E: Preliminary data taken for comparison to data taken by Finio

Air Flow Rate (scfm)	Pressure Reading (%)	Flow Rate-Orifice (lb/s)	Flow Rate-Orifice (gpm)	Pressure Air In (psi)	Density (lbm/ft^3)	Air Flow Rate (cfm)
18.5	35.8	4.06	29.25	10	0.124	31.27
15	33.4	3.92	28.25	10	0.124	25.36
6.5	16.5	2.76	19.85	10	0.124	10.99
5	12	2.35	16.93	10	0.124	8.45
10	22.4	3.21	23.13	10	0.124	16.90
15	31.1	3.78	27.26	10	0.124	25.36
20	37.1	4.13	29.77	10	0.124	33.81
26	43.2	4.46	32.13	15	0.150	52.92
20	38.9	4.23	30.49	16	0.155	42.09
15	33.4	3.92	28.25	15	0.150	30.53
10	26.5	3.49	25.16	15	0.150	20.36
5	15.1	2.64	18.99	15	0.150	10.18
12	29.2	3.67	26.41	15	0.150	24.43
17	36.3	4.09	29.45	15	0.150	34.60
22	41	4.35	31.30	15	0.150	44.78
25	43.2	4.46	32.13	15	0.150	50.89
28.5	48.3	4.72	33.97	20	0.175	67.85
23	41.8	4.39	31.60	20	0.175	54.76
18	39.3	4.25	30.64	20	0.175	42.85
13	31.9	3.83	27.61	20	0.175	30.95
8	22.5	3.22	23.19	20	0.175	19.05
4	12.4	2.39	17.21	20	0.175	9.52
10	25.4	3.42	24.63	20	0.175	23.81
15	35.5	4.04	29.12	20	0.175	35.71
20	39.1	4.24	30.56	20	0.175	47.62
25	43.9	4.50	32.39	20	0.175	59.52
30	49.6	4.78	34.42	25	0.201	81.78
25	44.5	4.53	32.61	25	0.201	68.15
20	42.5	4.42	31.87	25	0.201	54.52
15	35.1	4.02	28.96	25	0.201	40.89
10	28.9	3.65	26.28	25	0.201	27.26
5	18.8	2.94	21.19	25	0.201	13.63
8	24.1	3.33	24.00	25	0.201	21.81
18	40.5	4.32	31.11	25	0.201	49.07
5	17.3	2.82	20.33	30	0.226	15.36
12	32.9	3.89	28.04	30	0.226	36.85
17	38.5	4.21	30.33	30	0.226	52.21

22	45.8	4.59	33.08	30	0.226	67.57
27	47.1	4.66	33.55	30	0.226	82.92
32	52.2	4.90	35.31	30	0.226	98.28

Table 2E: Data on the effects of auxiliary water swirl

Air Flow Rate (cfm)	Pressure Reading (%)	Flow Rate-Orifice (lb/s)	Flow Rate-Orifice (gpm)	Pressure Air In (psi)	Angle of 4" Valve (°)	Aux. Pump (gpm)	Net Water Out (gpm)
Spiral Nozzle							
20	29.2	3.67	26.41	20	60	0	26.41
20	27.9	3.58	25.82	20	60	2	23.82
20	25	3.39	24.44	20	60	4.5	19.94
20	23	3.25	23.44	20	60	10	13.44
20	6.8	1.77	12.75	20	75	10	2.75
20	6.7	1.76	12.65	20	75	5	7.65
20	6.9	1.78	12.84	20	75	1.25	11.59
20	7.6	1.87	13.47	20	75	0	13.47
10	7	1.80	12.93	20	75	7.1	5.83
20	5.8	1.63	11.77	20	75	0	11.77
20	5.4	1.58	11.36	20	75	3	8.36
20	6	1.66	11.97	30	75	3	8.97
20	6.1	1.68	12.07	30	75	0	12.07
20	3.9	1.34	9.65	30	75	17.6	-7.95
Straight Nozzle							
20	11.1	1.37	9.87	20	75	0	9.87
20	10.9	1.36	9.78	20	75	1	8.78
20	10.3	1.32	9.51	20	75	3.25	6.26
20	10	1.30	9.37	20	75	5.5	3.87
20	9.9	1.29	9.33	20	75	7.5	1.83
20	9.1	1.24	8.94	20	75	8.75	0.19
20	7.5	1.13	8.12	20	75	17.6	-9.48

Table 3E: Swirl nozzle data

Air Flow Rate (cfm)	Pressure Reading (%)	Flow Rate-Orifice (lb/s)	Flow Rate-Orifice (gpm)	Pressure Air In (psi)	Angle Valve (°)	Density (lbm/ft³)	Air Flow (cfm)	Flow Ratio (gpm /cfm)
5	4.6	1.46	10.48	10	60	0.123	8.47	1.24
5	1.3	0.77	5.57	10	75	0.123	8.47	0.66
10	3	1.18	8.47	10	75	0.123	16.94	0.50
15	4.6	1.46	10.48	10	75	0.123	25.41	0.41
20	5.5	1.59	11.46	10	75	0.123	33.87	0.34
28	6.8	1.77	12.75	20	75	0.174	66.85	0.19
15	4.8	1.49	10.71	20	75	0.174	35.81	0.30
10	3.7	1.31	9.40	20	75	0.174	23.87	0.39
5	1.8	0.91	6.56	20	75	0.174	11.94	0.55
5	2.6	1.09	7.88	30	75	0.224	15.41	0.51
10	4.1	1.37	9.90	30	75	0.224	30.81	0.32
15	5.1	1.53	11.04	30	75	0.224	46.22	0.24
20	5.9	1.65	11.87	30	75	0.224	61.62	0.19
25	6.4	1.72	12.37	30	75	0.224	77.03	0.16
32	7.3	1.83	13.21	30	75	0.224	98.59	0.13
5	9.93	2.14	15.40	10	60	0.125	8.41	1.83
10	16.6	2.76	19.91	10	60	0.125	16.82	1.18
15	19.9	3.03	21.80	10	60	0.125	25.23	0.86
19	23.8	3.31	23.85	10	60	0.125	31.95	0.75
28	31.5	3.81	27.43	20	60	0.175	66.18	0.41
20	26.7	3.51	25.26	20	60	0.175	47.27	0.53
15	24	3.32	23.95	20	60	0.175	35.45	0.68
10	17.1	2.81	20.21	20	60	0.175	23.64	0.86
5	10.9	2.24	16.14	20	60	0.175	11.82	1.37
5	13.1	2.46	17.69	30	60	0.226	15.23	1.16
10	19	2.96	21.31	30	60	0.226	30.45	0.70
15	25.6	3.43	24.73	30	60	0.226	45.68	0.54
20	28.5	3.62	26.09	30	60	0.226	60.91	0.43
32	34.1	3.96	28.54	30	60	0.226	97.46	0.29
32	49.4	4.77	34.35	30	45	0.226	97.46	0.35
25	46.2	4.61	33.22	30	45	0.226	76.14	0.44
20	43.1	4.46	32.09	30	45	0.226	60.91	0.53
15	36.3	4.09	29.45	30	45	0.226	45.68	0.64
10	30.4	3.74	26.95	30	45	0.226	30.45	0.88
5	18.2	2.90	20.85	30	45	0.226	15.23	1.37
5	16.2	2.73	19.67	20	45	0.175	11.82	1.66
10	26.7	3.51	25.26	20	45	0.175	23.64	1.07

15	34.5	3.99	28.71	20	45	0.175	35.45	0.81
20	39	4.24	30.52	20	45	0.175	47.27	0.65
28	46.8	4.64	33.44	20	45	0.175	66.18	0.51
20	35.1	4.02	28.96	10	45	0.125	33.64	0.86
15	31.2	3.79	27.30	10	45	0.125	25.23	1.08
10	23.6	3.30	23.75	10	45	0.125	16.82	1.41
5	12.1	2.36	17.00	10	45	0.125	8.41	2.02

Table 4E: Straight nozzle data

Air Flow (scfm)	Pressure Reading (%)	Flow Rate-Orifice (lb/s)	Flow Rate-Orifice (gpm)	Pressure Air In (psi)	Valve Angle (deg)	Aux Pump (gpm)	Density (lbm/ft^3)	Air Flow (cfm)	Flow Ratio (gpm/cfm)
5	7.9	1.91	13.74	10	0	0	0.131	8.40	1.64
10	24	3.32	23.95	10	0	0	0.131	16.80	1.43
15	28.8	3.64	26.23	10	0	0	0.131	25.20	1.04
20	38.3	4.20	30.25	10	0	0	0.131	33.60	0.90
28	45.3	4.57	32.90	20	0	0	0.184	66.08	0.50
25	46.7	4.64	33.40	20	0	0	0.184	59.00	0.57
20	41.4	4.37	31.45	20	0	0	0.184	47.20	0.67
15	34.9	4.01	28.88	20	0	0	0.184	35.40	0.82
10	26	3.46	24.92	20	0	0	0.184	23.60	1.06
5	12.4	2.39	17.21	20	0	0	0.184	11.80	1.46
5	20.1	3.04	21.91	30	0	0	0.236	15.20	1.44
10	29.1	3.66	26.37	30	0	0	0.236	30.40	0.87
15	37.4	4.15	29.89	30	0	0	0.236	45.60	0.66
20	45	4.55	32.79	30	0	0	0.236	60.80	0.54
25	48.8	4.74	34.15	30	0	0	0.236	76.00	0.45
32	51.8	4.88	35.18	30	0	0	0.236	97.28	0.36
32	51.9	4.89	35.21	30	45	0	0.236	97.28	0.36
30	50	4.80	34.56	30	45	0	0.236	91.20	0.38
25	48.9	4.75	34.18	30	45	0	0.236	76.00	0.45
20	43.1	4.46	32.09	30	45	0	0.236	60.80	0.53
15	38	4.18	30.13	30	45	0	0.236	45.60	0.66
10	27.3	3.55	25.54	30	45	0	0.236	30.40	0.84
5	16.9	2.79	20.09	30	45	0	0.236	15.20	1.32
5	14.5	2.58	18.61	20	45	0	0.184	11.80	1.58
10	24.4	3.35	24.14	20	45	0	0.184	23.60	1.02
15	35.2	4.03	29.00	20	45	0	0.184	35.40	0.82
20	41.3	4.36	31.41	20	45	0	0.184	47.20	0.67
25	43.9	4.50	32.39	20	45	0	0.184	59.00	0.55
28	44	4.50	32.42	20	45	0	0.184	66.08	0.49
19	35.4	4.04	29.08	10	45	0	0.131	31.92	0.91
15	30.1	3.72	26.82	10	45	0	0.131	25.20	1.06
10	20.4	3.06	22.08	10	45	0	0.131	16.80	1.31
5	7.8	1.90	13.65	10	45	0	0.131	8.40	1.63
20	22.9	3.25	23.39	10	60	0	0.131	33.60	0.70

15	20.6	3.08	22.18	10	60	0	0.131	25.20	0.88
10	14.9	2.62	18.87	10	60	0	0.131	16.80	1.12
5	6.5	1.73	12.46	10	60	0	0.131	8.40	1.48
5	9.2	2.06	14.83	20	60	0	0.184	11.80	1.26
10	16.4	2.75	19.79	20	60	0	0.184	23.60	0.84
15	21.7	3.16	22.77	20	60	0	0.184	35.40	0.64
20	25.5	3.43	24.68	20	60	0	0.184	47.20	0.52
28	29.1	3.66	26.37	20	60	0	0.184	66.08	0.40
33	32.6	3.87	27.91	30	60	0	0.236	100.32	0.28
30	31.3	3.80	27.35	30	60	0	0.236	91.20	0.30
25	29.5	3.69	26.55	30	60	0	0.236	76.00	0.35
20	28.4	3.62	26.05	30	60	0	0.236	60.80	0.43
15	24.6	3.37	24.24	30	60	0	0.236	45.60	0.53
10	19.8	3.02	21.75	30	60	0	0.236	30.40	0.72
5	11.9	2.34	16.86	30	60	0	0.236	15.20	1.11
32	10.3	2.18	15.69	30	75	0	0.236	97.28	0.16
25	10.4	2.19	15.76	30	75	0	0.236	76.00	0.21
20	9.7	2.11	15.22	30	75	0	0.236	60.80	0.25
15	7.4	1.85	13.30	30	75	0	0.236	45.60	0.29
10	5.9	1.65	11.87	30	75	0	0.236	30.40	0.39
5	3.9	1.34	9.65	30	75	0	0.236	15.20	0.64
28	8.5	1.98	14.25	20	75	0	0.184	66.08	0.22
25	8	1.92	13.83	20	75	0	0.184	59.00	0.23
20	7.5	1.86	13.39	20	75	0	0.184	47.20	0.28
15	6.3	1.70	12.27	20	75	0	0.184	35.40	0.35
10	5	1.52	10.93	20	75	0	0.184	23.60	0.46
5	3.8	1.32	9.53	20	75	0	0.184	11.80	0.81
20	7.3	1.83	13.21	10	75	0	0.131	33.60	0.39
15	6.8	1.77	12.75	10	75	0	0.131	25.20	0.51
10	5.2	1.55	11.15	10	75	0	0.131	16.80	0.66
5	2.7	1.12	8.03	10	75	0	0.131	8.40	0.96

Table 5E: L_{eq}/D analysis

Flow Rate- Orifice (gpm)	Valve Angle (deg)	Density (lbm/ft³)	Air Flow (cfm)	Nozzle	f	Leq/D	Flow Ratio (gpm/cfm)
10.93	75	0.184	23.60	Straight	0.001	2.1E+06	0.463
19.79	60	0.184	23.60	Straight	0.002	1.3E+05	0.839
24.14	45	0.184	23.60	Straight	0.002	1.7E+04	1.023
24.92	0	0.184	23.60	Straight	0.002	2.2E+03	1.056
12.75	75	0.131	25.20	Straight	0.001	2.1E+06	0.506
22.18	60	0.131	25.20	Straight	0.002	1.3E+05	0.880
26.82	45	0.131	25.20	Straight	0.003	1.1E+04	1.064
26.23	0	0.131	25.20	Straight	0.003	1.5E+03	1.041
10.48	75	0.123	25.41	Swirl	0.001	2.1E+06	0.413
21.80	60	0.125	25.23	Swirl	0.002	1.3E+05	0.864
27.30	45	0.125	25.23	Swirl	0.003	1.1E+04	1.082
28.25	0	0.124	25.36	Swirl	0.003	1.5E+03	1.114
9.40	75	0.174	23.87	Swirl	0.001	2.1E+06	0.394
20.21	60	0.175	23.64	Swirl	0.002	1.3E+05	0.855
25.26	45	0.175	23.64	Swirl	0.002	1.7E+04	1.069
24.63	0	0.175	23.81	Swirl	0.002	2.2E+03	1.035

Table 6E: Additional data used for L_{eq}/D analysis

Angle From Fully Open	0	45	60	75
K-4" valve (from emperical relation)	0.05	29.39	246.23	2062.69
K-tot	4.09	33.43	250.27	2066.73
L- Regular (ft)	10.92	x	x	x
L- Backflow (ft)	32.67	x	x	x
L- total (ft)	43.59	x	x	x
Diameter (ft)	0.333	x	x	x
Lactual/D	130.9	x	x	x